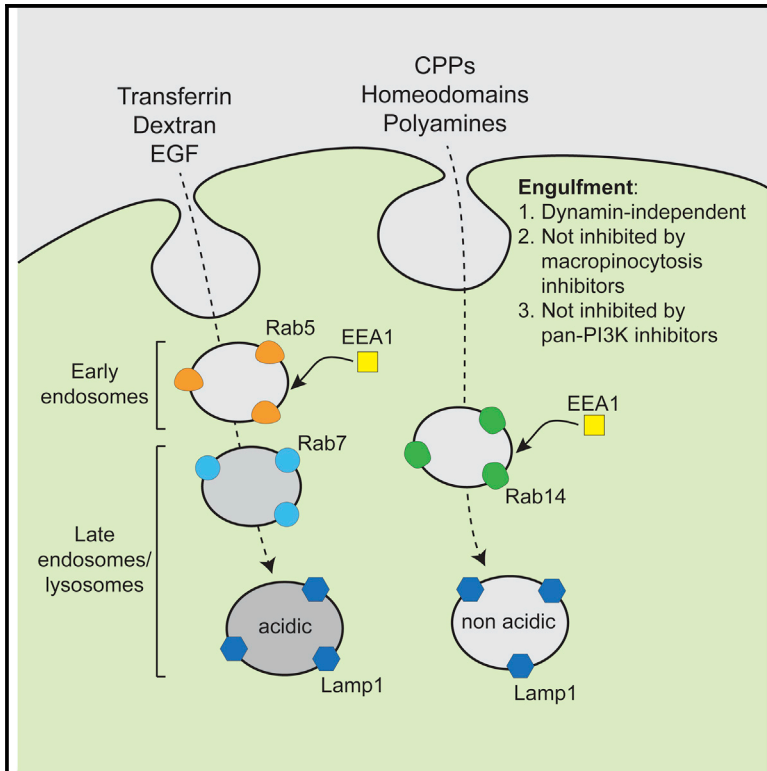


The endocytic pathway taken by cationic substances requires Rab14 but not Rab5 and Rab7

Graphical abstract



Authors

Evgeniya Trofimenko, Yuta Homma, Mitsunori Fukuda, Christian Widmann

Correspondence

Christian.Widmann@unil.ch

In brief

Cells can engulf material brought to acidic degradative vesicles marked with the Lamp1 protein. Trofimenko et al. identify an endocytic pathway moving cationic substances to Lamp1-positive vesicles that are non-acidic and probably nondegradative. This pathway requires Rab14, unlike classical endocytosis that is regulated by Rab5 and Rab7.

Highlights

- Cationic substances use the Rab14-dependent endocytic pathway
- Inhibitors of classical endocytosis do not prevent cationic peptide endocytosis
- Cationic substances end up in non-acidic Lamp1 compartments



Article

The endocytic pathway taken by cationic substances requires Rab14 but not Rab5 and Rab7

Evgeniya Trofimenko,¹ Yuta Homma,² Mitsunori Fukuda,² and Christian Widmann^{1,3,*}¹Department of Biomedical Sciences, University of Lausanne, Lausanne, Switzerland²Laboratory of Membrane Trafficking Mechanisms, Department of Integrative Life Sciences, Graduate School of Life Sciences, Tohoku University, Sendai, Miyagi, Japan³Lead contact*Correspondence: Christian.Widmann@unil.ch<https://doi.org/10.1016/j.celrep.2021.109945>**SUMMARY**

Endocytosis and endosome dynamics are controlled by proteins of the small GTPase Rab family. Besides possible recycling routes to the plasma membrane and various organelles, previously described endocytic pathways (e.g., clathrin-mediated endocytosis, macropinocytosis, CLIC/GEEC pathway) all appear to funnel the endocytosed material to Rab5-positive early endosomes that then mature into Rab7-positive late endosomes/lysosomes. By studying the uptake of a series of cell-penetrating peptides (CPPs), we identify an endocytic pathway that moves material to nonacidic Lamp1-positive late endosomes. Trafficking via this endocytic route is fully independent of Rab5 and Rab7 but requires the Rab14 protein. The pathway taken by CPPs differs from the conventional Rab5-dependent endocytosis at the stage of vesicle formation already, as it is not affected by a series of compounds that inhibit macropinocytosis or clathrin-mediated endocytosis. The Rab14-dependent pathway is also used by physiological cationic molecules such as polyamines and homeodomains found in homeoproteins.

INTRODUCTION

Endocytosis is a major entry route used by cells to take up a variety of extracellular substances ranging from nutrients, fluid phase material, growth factors, hormones, receptors, cellular penetrating peptides (CPPs), viruses or bacteria. Various forms of endocytosis have been described, the main routes being clathrin-mediated endocytosis, macropinocytosis, and the clathrin-independent carrier/glycosylphosphatidylinositol-anchored protein enriched endocytic compartment (CLIC/GEEC) pathway (reviewed in Johannes et al. [2015], Kaksonen and Roux [2018], Mercer et al. [2010], Schmid et al. [2014], and Thottacherry et al. [2019]). Which form of endocytosis is used and the ultimate fate of the endocytosed material depend on the nature of the substances being taken up by cells.

Endocytic vesicles (endosomes) are formed by membrane invaginations, actin-driven membrane protrusions (in the case of macropinocytosis for example), or ruffling. For clathrin-mediated endocytosis, vesicle formation can be triggered through the detection of the endosomal cargo by AP2 adaptor domains and subsequent recruitment of clathrin triskelions (Cocucci et al., 2012; Takei and Haucke, 2001). Several AP2 adaptors bound to the plasma membrane through PI(4,5)P₂ are necessary for efficient clathrin binding (Cocucci et al., 2012). Accumulation of AP2/clathrin complexes (within seconds) at the membrane leads to membrane bending and endocytic vesicle formation (Chen and Schmid, 2020; Cocucci et al., 2012; Takei and Haucke, 2001).

Endosomes are dynamic structures that undergo fusion and fission events (Gautreau et al., 2014). Early endosomes mature into multivesicular bodies (MVBs), late endosomes, and finally lysosomes, where degradation of the endocytosed material occurs (Huotari and Helenius, 2011; Scott et al., 2014). The endocytosed material can also be recycled back to the plasma membrane or trafficked toward other cellular compartments (Huotari and Helenius, 2011; Naslavsky and Caplan, 2018; Scott et al., 2014).

Each stage of endosomal maturation is finely controlled by the sequential recruitment of various endosomal proteins and lipids. For example, on early endosomes, Rab5, activated by its guanine exchange factor (GEF) Rabex-5, controls local generation of PI(3)P by recruiting the Vps34 PI3 kinase. This in turn, leads to recruitment of EEA1 via its capacity to bind PI(3)P through its FYVE domain. EEA1 can also directly interact with the active GTP-bound form of Rab5. The ability of EEA1 to bind simultaneously Rab5 and PI(3)P on separate vesicles makes it a tethering protein that contributes to endosomal fusion (Murray et al., 2016). Vps34 knockout in mammalian cells leads to enlarged early endosomes and interruption of the progression of endocytosed cargo to lysosomes (Jaber et al., 2016). Vesicle maturation proceeds through the recruitment of the Mon1-Ccz1 complex that interacts with Rab5 and PI(3)P. The Mon1-Ccz1 complex has a GEF activity toward Rab7 that leads to the activation of this small GTPase on endosomes [reviewed in Huotari and Helenius (2011), and Langemeyer et al. (2018)]. Concomitantly, Rab5 GTPase-activating protein (GAP) turns off Rab5 and



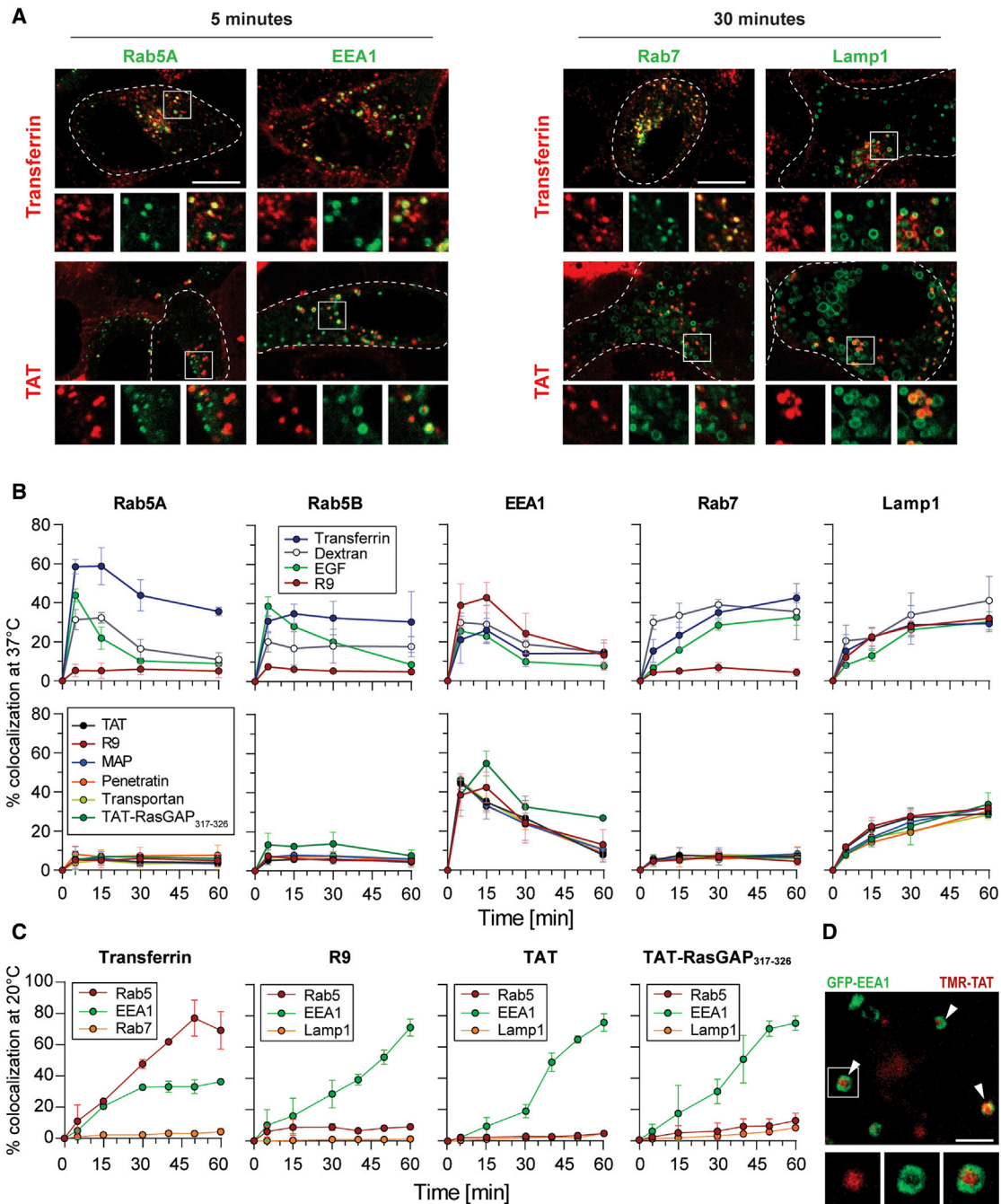


Figure 1. Rab5 and Rab7 are mostly absent from CPP-containing endosomes

(A–D) HeLa KCNN4 knockout cells ectopically expressing early (Rab5A, Rab5B and EEA1) or late (Rab7 and Lamp1) endosomal markers were incubated with 20 μ g/ml AlexaFluor568-transferrin, 0.2 mg/ml TMR-10 kDa dextran, 2 μ g/ml AlexaFluor647-EGF or with 40 μ M of TMR- (TAT, R9, Penetratin, TAT-RasGAP₃₁₇₋₃₂₆) or FITC-labeled (MAP, Transportan) CPPs for 5 min, then washed and imaged at the indicated time points by confocal microscopy (see Figure S1D for experimental setup). All experiments were performed on live cells at 37°C unless indicated otherwise.

(A) Representative confocal images of HeLa KCNN4 knockout cells, expressing GFP-tagged endosomal markers, incubated with AlexaFluor568-transferrin or TMR-TAT. Images were acquired at 5 or 30 min after the addition of the cargos. Scale bar: 10 μ m.

(B and C) Quantitation of colocalization between the indicated fluorescent material and fluorescently tagged early and late endosomal markers. Colocalization analysis was performed as described in the Methods and Figure S1B–C. The data correspond to the mean \pm SD of three independent experiments. In (B), the data

(legend continued on next page)

promotes the release of the latter from early endosomes. Hence, Rab5 and Rab7 regulate essential steps in the endocytic pathway that moves endocytosed material to lysosome. The Rab5/Rab7-controlled endocytic pathway is currently the only molecularly characterized route taken by endocytosed material that ends up in lysosomes (Langemeyer et al., 2018; Mercer et al., 2010; Thottacherry et al., 2019).

In this study we show that endocytosed CPPs, homeodomain, and polyamines, follow an endosomal pathway that requires Rab14 but not Rab5 or Rab7 for EEA1 recruitment on early endosomes and maturation of the vesicles toward nonacidic Lamp1-positive late endosomes. Endocytosis of CPPs is also unaffected by phosphoinositide 3-kinase (PI3K) inhibitors or various pharmacological agents known to inhibit the uptake of classical cargos such as transferrin and dextran. This work therefore defines a second independent endocytic maturation pathway that moves endocytosed material to Lamp1-positive vesicles.

RESULTS

CPPs are not taken up by cells by classical endocytosis

CPPs can be used for transport of bioactive cargo into cells (Bechara and Sagan, 2013; Futaki et al., 2013; Guidotti et al., 2017; Illien et al., 2016; Jones and Sayers, 2012; Koren and Torchilin, 2012; Kristensen et al., 2016; Madani et al., 2011; Mueller et al., 2008; Ruseska and Zimmer, 2020; Trabulo et al., 2010; Vasconcelos et al., 2013; Xie et al., 2020). Various non-exclusive mechanisms of CPP endocytosis have been proposed (Bechara and Sagan, 2013; Cleal et al., 2013; Futaki et al., 2013; Futaki and Nakase, 2017; Guidotti et al., 2017; Jones and Sayers, 2012; Koren and Torchilin, 2012; Madani et al., 2011; Räägel et al., 2010; Ruseska and Zimmer, 2020; Trabulo et al., 2010; Vasconcelos et al., 2013). However, there is no consensus and clarity regarding the precise nature of the endosomal pathway used by CPPs and its underlying mechanisms. CPPs additionally enter cells through direct translocation (Bechara and Sagan, 2013; Futaki et al., 2013; Guidotti et al., 2017; Jones and Sayers, 2012; Koren and Torchilin, 2012; Madani et al., 2011; Ruseska and Zimmer, 2020; Trabulo et al., 2010; Vasconcelos et al., 2013). We have recently demonstrated that direct translocation of cationic CPPs can occur via water pores that are formed as a consequence of membrane megapolarization induced by the CPPs themselves and the activity of potassium channels (Trofimenko et al., 2021). Direct translocation can be inhibited through plasma membrane depolarization (Chaloin et al., 1998; Rothbard et al., 2004; Trofimenko et al., 2021; Wallbrecher et al., 2017; Zhang et al., 2009) or inactivation of specific potassium channels (e.g., KCNN4 in HeLa cells) (Trofimenko et al., 2021), without affecting endocytosis of CPPs (Trofimenko et al., 2021), transferrin (Torriani et al., 2019) or vesicular stomatitis virus (VSV) (Torriani et al., 2019). Here, we took advantage of KCNN4 knockout

HeLa cells to study endocytosis in cells in which CPP direct translocation in the cytosol is strongly reduced, therefore allowing for facilitated visualization of CPP endocytic vesicles. Unless otherwise mentioned, these are the cells that were used in the presented experiments. To investigate the endocytic pathway employed by CPPs, we phenotypically characterized CPP-containing vesicles (Figure S1) for the presence of early (Rab5 and EEA1) and late (Rab7 and Lamp1) endosomal markers. We selected five most commonly used CPPs in research and in clinic (TAT, R9, Penetratin, MAP and Transportan) as well as TAT-Ras-GAP₃₁₇₋₃₂₆, a prototypical TAT-cargo complex (Annibaldi et al., 2011; Barras et al., 2014a; Barras et al., 2014b; Chevalier et al., 2015; Heulot et al., 2016; Heulot et al., 2017; Michod et al., 2009; Michod et al., 2004; Pittet et al., 2007; Serulla et al., 2020; Trofimenko et al., 2021; Tsoutsou et al., 2017; Figure S1A). Pulse-chase experiments (Figures 1A, 1B, and S1D) demonstrated colocalization of transferrin, EGF and dextran with EEA1, Rab5A and Rab5B at early time points, and Rab7 and Lamp1 at later time points. These results are consistent with previous knowledge that these molecules enter cells through clathrin-mediated endocytosis (transferrin and EGF) and macropinocytosis (dextran). Ectopic expression of endosomal markers did not interfere with normal endocytosis, as the pattern of EEA1-positive and Lamp1-positive vesicles was found to be qualitatively similar in control cells and in cells expressing GFP-tagged versions of these markers (Figure S2A). Moreover, ectopic expression of the tagged EEA1 and Lamp1 constructs did not alter the kinetics of transferrin colocalization with EEA1- or Lamp1-positive vesicles (Figure S2B). These results indicate that ectopic expression of fluorescent endosomal markers—in live cells in particular—does not appear to affect endocytic processes. CPPs were found in EEA1- and Lamp1-positive vesicles at early and late time points, respectively (Figures 1A and 1B), but surprisingly, only a minority of CPP-containing vesicles were positive for Rab5 and Rab7 (Figures 1A, 1B, S1B, and S1C). These data were confirmed in wild-type HeLa cells (Figures S2C–S2F), demonstrating that KCNN4 depletion did not interfere with endocytosis. Furthermore, TAT internalization occurred similarly at 1 or 40 μ M or whether the peptide was synthesized with L or D amino acids (Figures 1B, S2E, and S2F). The CPPs investigated in the present work all carry positive charges (Figure S1A) and, despite having otherwise different physicochemical properties, colocalized within the same endocytic vesicles (Figure S2G).

The association of Rab5 with CPP-containing vesicles could be very transient, making it hard to visualize. We therefore performed experiments at 20°C to slow down endosomal maturation as can be observed for transferrin-containing vesicles (Figure 1C, left). In this setting, CPP-positive endosomes remained mostly Rab5-negative (Figure 1C). Additionally, Rab5- and Rab7-positive CPP-containing vesicles were only marginally detected in the continuous presence of the CPPs despite extensive

obtained with R9 are shown, for comparison, both on the top graphs and the bottom graphs. In (C), cells were incubated at 20°C to delay endosomal maturation (155–180 cells were analyzed per condition).

(D) Representative confocal, Airyscan acquired, high-resolution images of cells ectopically expressing GFP-EEA1 incubated with 40 μ M TMR-TAT for 5 min. Scale bar: 2 μ m.

See also Figures S1–S3.

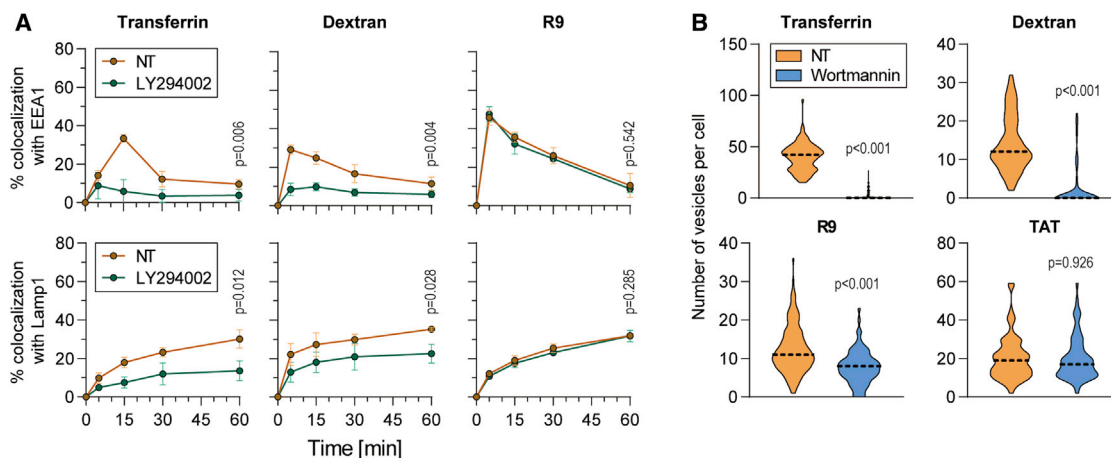


Figure 2. CPP endocytosis does not require PI(3)P-kinase-like enzymes

(A) Colocalization quantitation between the indicated endosomal material and endosomal markers in the presence or in the absence of LY294002, a pan-PI3-kinase inhibitor. HeLa KCNN4 knockout cells, ectopically expressing GFP-tagged EEA1 or Lamp1, were incubated or not for 30 min with 25 μ M LY294002 in RPMI without serum. The cells were then incubated for a 5-minute pulse in RPMI, 10% FBS with either 20 μ g/ml AlexaFluor568-transferrin, 0.2 mg/ml TMR-10 kDa dextran or 40 μ M TMR-R9, washed, and then visualized by confocal microscopy over time (time 0 corresponds to the addition of the cargos). When used, LY294002 was maintained in the media throughout the full duration of the experiment. The data correspond to the mean \pm SD of 160 cells (per condition) sampled from three independent experiments. The p values were calculated on area under the curve (AUC) values using parametric unpaired two-tailed t tests.

(B) Quantitation of the number of endosomal vesicles per cell in the presence or in the absence of wortmannin, a pan-PI3-kinase inhibitor. HeLa KCNN4 knockout cells were incubated with 20 μ g/ml AlexaFluor568-transferrin, 0.2 mg/ml TMR-10 kDa dextran or 40 μ M TMR-CPP for a pulse of 5 min. Cells were preincubated or not for 30 min with 10 μ M wortmannin, which was still present during the full duration of the experiment. The number of vesicles positive for the indicated endosomal material were visually counted from confocal images, acquired in the middle of the cell. The results are derived from the analysis of 160 cells (per condition) taken from three independent experiments. The p values were calculated using parametric paired two-tailed t test.

See also Figure S4.

colocalization with EEA1 (Figure S2H). High resolution confocal images showed that TAT was found inside EEA1-positive vesicles already a few minutes after being added to cells (Figure 1D), confirming that CPPs are indeed located in EEA1-positive endosomes. TAT-RasGAP₃₁₇₋₃₂₆ did not interfere with the progression of transferrin through early and late endosomes (Figure S2I) and did not lead to the generation of aberrant endosomes bearing EEA1 and Lamp1 at the same time (Figure S2J). This indicates that CPPs do not reprogram the manner by which cells take up material through classical endocytosis. Lack of colocalization with Rab5A and Rab7 was observed previously for the tryptophane/arginine-rich WRAP peptide linked to siRNA (De-shayes et al., 2020). Additionally, based on visual inspection of representative images in the literature, R8 and TAT also colocalize only partially with Rab5A (Appelbaum et al., 2012).

Pharmacological agents such as EIPA (Koivusalo et al., 2010), IPA3 (Dharmawardhane et al., 2000; Viaud and Peterson, 2009), ML7 (Araki et al., 2003; Bain et al., 2003), Jasplakinolide (Bubb et al., 1994), and Cytochalasin D (Fujimoto et al., 2000; Sampath and Pollard, 1991) block various events linked to macropinosome formation and maturation. EIPA is a sodium-proton exchange inhibitor. IPA3 is a PAK1 inhibitor. Jasplakinolide and cytochalasin D interfere positively and negatively, respectively, with actin filament polymerization and ML7 prevents macropinosome formation and closure. We observed no effect of these inhibitors on the internalization of TAT-RasGAP₃₁₇₋₃₂₆ in contrast to what was seen for dextran uptake (Figures S3A and S3B). Additionally, as opposed to transferrin internalization, the early

stages of CPP endocytosis were dynamin-independent (Figures S3C and S3D).

Lipids such as phosphoinositides (PIs) that can be phosphorylated at positions 3, 4, or 5 of the inositol ring, represent another type of endocytosis markers. For example, PI(4,5)P₂ is enriched in the plasma membrane, whereas PI(3)P and PI(3,5)P₂ are enriched in early and late endosomes, respectively, and participate in their formation [reviewed in Bissig et al. (2012), Campa et al. (2015), Miaczynska and Zerial (2002), Ramadani et al. (2010), and Wenk and De Camilli (2004)]. In conventional endocytosis, EEA1 is recruited to early endosomes through interactions with Rab5 and PI(3)P (McBride et al., 1999; Simonsen et al., 1998; Zeigerer et al., 2012). The latter is produced by Vps34, a PI3-kinase that is also recruited by Rab5. We therefore used pan-PI3K inhibitors (wortmannin and LY294002) (Figure S4A) and assessed the colocalization between selected endosomal material and EEA1 or Lamp1. LY294002 halted transferrin and dextran endosomal maturation and progression, consistent with observations reported in the literature (Fili et al., 2006; Jaber et al., 2016; Figure 2A). However, colocalization between CPPs and EEA1 or Lamp1 was not affected (Figure 2A). This suggests that EEA1 recruitment to CPP-positive vesicles differs from classical endocytosis and can occur at least in part, in a PI3K-independent manner.

Depletion of PI(3,4)P₂ blocks the fission of clathrin-coated vesicles from the plasma membrane (Posor et al., 2013) and prevents macropinosome closure (Hasegawa et al., 2011; Maekawa et al., 2014). Wortmanin, at high micromolar concentrations,

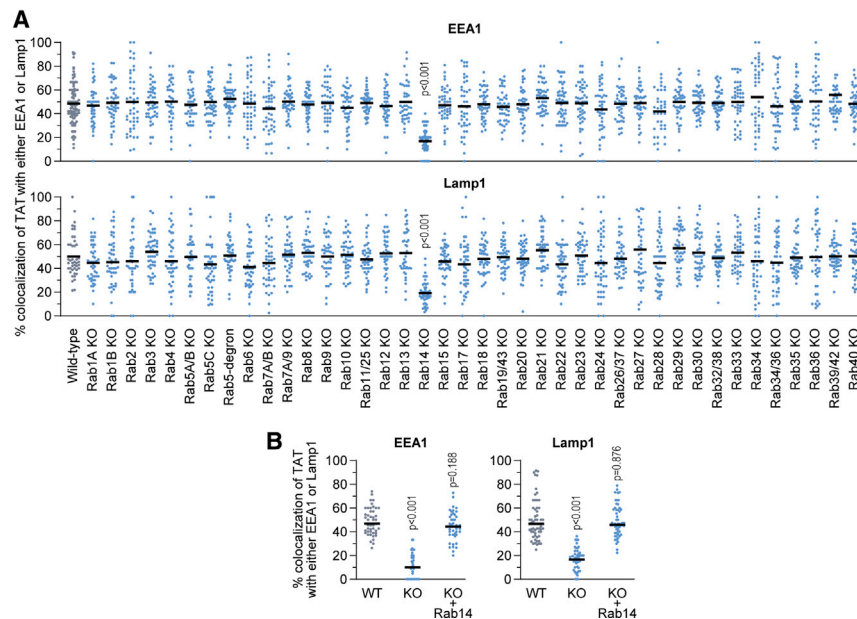


Figure 3. CPP endosomal maturation is Rab14-dependent

(A) Colocalization quantitation between TMR-TAT and GFP-EEA1 (15 min) or Lamp1-GFP (30 min) in a pulse-chase experiment performed in MDCK-II wild-type cells and the indicated Rab knockouts. A total of 50–65 cells were quantitated per condition. Statistical analysis was performed with ANOVA multiple comparison to the wild-type cell condition with Dunnett's correction. Only significant p values are shown. Rab5-degron cells were treated with 1 μ g/ml doxycycline and 500 μ M IAA for 48 h to induce degradation of degron-tagged Rab5A in the Rab5B/C knockout cell line (see Figure S5A). (B) Rab14 rescue experiment. Rab14 knockout cells were transiently transfected (KO + Rab14) or not (KO) with a GFP-Rab14 wild-type construct. These cells, along wild-type MDCK cells (WT), were then analyzed as in (A) (55–58 cells per condition were quantitated). See also Figures S5 and S6.

besides inducing PI(3)P depletion, inhibits PI4-kinases (Balla and Balla, 2006; Santos et al., 2013) and leads to depletion of PI(3,4)P₂ and PI(3,4,5)P₃ (Gozzelino et al., 2020; Naguib, 2016; Zhang et al., 2017). As expected, wortmannin almost fully inhibited the endocytosis of transferrin and dextran (Figure 2B). In contrast, wortmannin had no or only minimal effect on the formation of TAT- or R9-containing endosomes (Figure 2B). Accordingly, formation and intracellular distribution of TMR-TAT-containing vesicles were not affected by wortmannin and LY294002 (Figure S4B).

As EEA1 binds PI(3)P, one could expect that wortmannin and LY294002 stimulate EEA1 translocation from endosomes to cytosol. This was however not observed for LY294002, and wortmannin only slightly induced this effect (Figures S4C and S4D). EEA1 can bind to endosomes via other means than PI(3)P though (e.g., by interacting with Rab proteins) and this can explain why phosphoinositide depletion does not lead to substantial EEA1 cytosolic translocation.

Even though previous studies have shown some contradictory results of CPP internalization in the presence of the endocytic inhibitors used in this study [decreased uptake (Appelbaum et al., 2012; Kaplan et al., 2005; Nakase et al., 2004; Wadia et al., 2004), no effect (Deshayes et al., 2020; Kawaguchi et al., 2016; Nakase et al., 2004; Polyakov et al., 2000), increased uptake (Duchardt et al., 2007)], our data clearly indicate that CPPs enter cells through an endocytic pathway, which differs from classical endocytosis already at the stage of endocytic vesicle formation.

Rab14 is required for the maturation of CPP-containing endosomes

The results presented above suggest that Rab5 is not involved in the endocytic pathway taken by CPPs. To exhaustively assess the role of Rab family members in CPP endocytosis, we took advantage of a knockout Rab library in MDCK cells consisting

of single and multiple knockouts (> 50 cell lines) targeting either different protein isoforms or multiple Rab proteins simultaneously (Homma et al., 2019). This library includes a Rab5 conditional knockout cell line, where Rab5A, B, and C isoforms have been knocked out and replaced by a Rab5A version that can be degraded through auxin-induced ubiquitination upon addition of indole-3-acetic acid (IAA) (Nishimura et al., 2009; Y.H., M.F., Y. Hatoyama, and S. Hiragi, unpublished data; Figure S5A). In MDCK cells, similarly to HeLa cells, there is a time-dependent colocalization of CPP-containing vesicles with EEA1 and Lamp1 but minimal colocalization with Rab5 and Rab7 (Figure S5B). As expected, transferrin-containing vesicle maturation was perturbed by Rab5 and Rab7 gene disruption in MDCK cells (Figure S5C). On the other hand, the recruitment of EEA1 (15 min post incubation), as well as Lamp1 acquisition (30 min post incubation) to TAT-containing vesicles was not affected by the absence of Rab5 isoforms (Figure 3A) or any other Rab family members except Rab14 (Figure 3A). Re-expressing Rab14 in the Rab14 knockout, MDCK cells restored the colocalization of CPPs with EEA1 and Lamp1 (Figure 3B). Absence of Rab14 had no effect on transferrin maturation to EEA1 and Lamp1-positive endosomes (Figure 5C). Colocalization of EEA1 with a series of CPPs was inhibited by Rab14 dominant-negative mutants both in wild-type and KCNN4 knockout HeLa cells (Figures 4A and S5D). However, Rab14 inhibition did not significantly affect the colocalization of EEA1 with transferrin or dextran (Figure 4A). EEA1 colocalization with mannose receptors (Weimershaus et al., 2018) or with EGF (Proikas-Cezanne et al., 2006) was also reported earlier not to be affected in Rab14-depleted cells. Rab14 was not required for the initial formation of CPP-containing endosomes (Figures S5E and S5F). The absence of Rab14 did not affect the number of EEA1-positive vesicles per cell (Figure S5G, left panel). In cells lacking Rab14, the EEA1 content of vesicles appeared to be slightly decreased although this did not

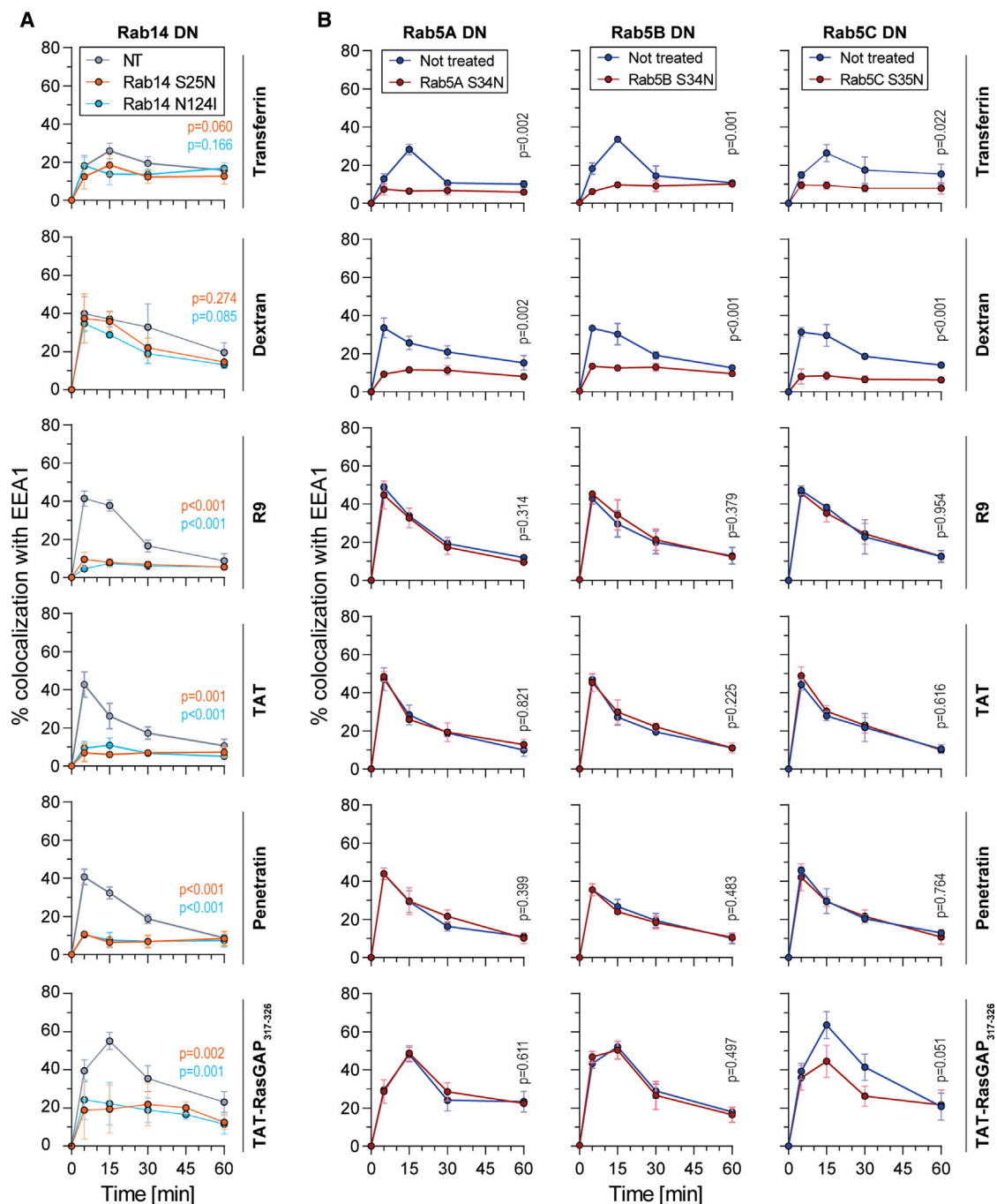


Figure 4. EEA1 acquisition on CPP-containing endosomes is Rab14-dependent but Rab5-independent

(A) Colocalization quantitation between the indicated endocytosed material and EEA1 in cells transfected with Rab14 dominant-negative constructs in HeLa KCNN4 knockout cells in a pulse chase experiment setting (see Figure S1D). The data correspond to the mean \pm SD of 150–170 analyzed cells per condition derived from three independent experiments. Statistical analysis was performed on AUC values using ANOVA test with Dunnett's correction. The p values correspond to the comparison with non-transfected (NT) cells.

(B) Colocalization quantitation of transferrin, dextran, and the indicated CPPs with EEA1 in cells transfected with the indicated Rab5 dominant-negative constructs using the same experimental setting as in (A). The data correspond to the mean \pm SD of 160–165 analyzed cells per condition derived from three independent experiments. Statistical analysis was performed using parametric two-tailed t test based on AUC values.

See also Figures S5 and S6.

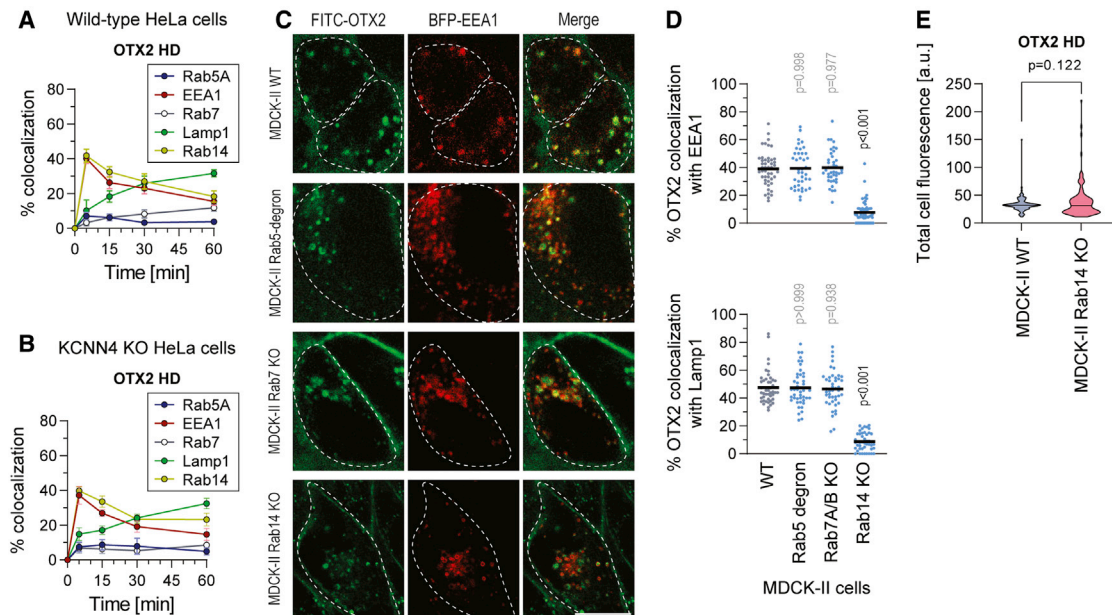


Figure 5. HDs are following a Rab5-independent, Rab14-dependent endocytic route

(A and B) Colocalization quantitation between endosomal markers and HD. Wild-type (A) and KCNN4 knockout (B) HeLa cells, ectopically expressing the indicated endosomal markers, were subjected to a 5-minute pulse incubation with fluorescently labeled OTX2 HD (10 μ M). Quantitation assessment was based on confocal images. The results correspond to the mean \pm SD of 150–170 analyzed cells per condition derived from three independent experiments. (C) Representative confocal images of the indicated MDCK-II cell lines expressing BFP-EEA1 incubated with 10 μ M FITC-OTX2 for a 5-min pulse. The images correspond to the 15 min time point. Scale bar: 10 μ m. (D) Colocalization quantitation between fluorescent versions of OTX2 HD (10 μ M) with EEA1 (top) or Lamp1 (bottom) in wild-type and the indicated Rab knockout MDCK-II cells. Cells were incubated for 5 min, then washed and confocal images were acquired at 15 and 30 min post incubation for early and late endosomal markers, respectively. A total of 54–60 cells per condition were analyzed. Statistical analysis was performed with ANOVA multiple comparison to wild-type condition with Dunett's correction. (E) Quantitation of total OTX2 HD uptake in MDCK-II wild-type and Rab14 knockout cells. Statistical analysis was done with parametric unpaired t test. A total of 130 cells per condition were analyzed.

reach statistical significance (Figure S5G, right panel). Taken together, these data support the role of Rab14 in maturation of CPP-containing endosomes but not in the initial formation of these vesicles.

The noninvolvement of Rab5 in the maturation of CPP-containing endosomes was further validated using Rab5 dominant-negative constructs (Rab5A S34N, Rab5B S34N or Rab5C S35N). These mutants, as expected, reduced the percentage of EEA1- or Lamp1-positive transferrin- and dextran-containing vesicles but had no significant effect on the percentage of EEA1- or Lamp1-positive CPP-containing vesicles (Figures 4B, S6A, and S6B).

Rab5 can recruit EEA1 on endosomes and conversely Rab5 dominant-negative mutants favors the release of EEA1 from endosomes (Dinneen and Ceresa, 2004; Johns et al., 2009; Mills et al., 1998; Sieczkarski and Whittaker, 2003; Zeigerer et al., 2012). Indeed, the number of EEA1-positive vesicles, as well as the EEA1 vesicle load, was significantly diminished by the Rab5C S35N mutant (Figures S6C and S6D, left and middle graphs, “Without CPP” conditions). The total cell-associated EEA1 signal was however not impacted by the Rab5 mutant (Figure S6D, right panel). Interestingly, CPPs counteracted the Rab5C S35N mutant-mediated decrease in the EEA1-positive vesicles

number and intensity (Figures S6C and S6D, left and middle graphs, “TAT” conditions), presumably because CPP-containing endosomes, which do not require Rab5 to acquire EEA1, capture some of the released EEA1 so that globally what is lost from classical endosomes is recovered on CPP-containing endosomes through the possible action of Rab14.

Homeoproteins and polyamines use the same endocytic pathway as CPPs

Homeoproteins (HPs) are a family of transcription factors involved in multiple biological processes (Di Nardo et al., 2018; Prochiantz and Di Nardo, 2015; Sagan et al., 2013; Spatazza et al., 2013). Additionally, HPs, such as Engrailed 2 and OTX2, exhibit therapeutic properties (Alvarez-Fischer et al., 2011; Blaudin de Thé et al., 2018; Rekaik et al., 2015a; Rekaik et al., 2015b; Sugiyama et al., 2008; Torero Ibad et al., 2011). The vast majority of HPs contain a conserved 60 amino-acids domain called the homeodomain (HD) that carries HP internalization and secretion motifs. Interestingly, the HP internalization motifs bear CPP sequences (Di Nardo et al., 2018; Spatazza et al., 2013). We therefore hypothesized that HDs could be endocytosed similarly as CPPs. Figures 5A and 5B show that there is substantial colocalization between the HD of OTX2 and the EEA1 or Lamp1 markers

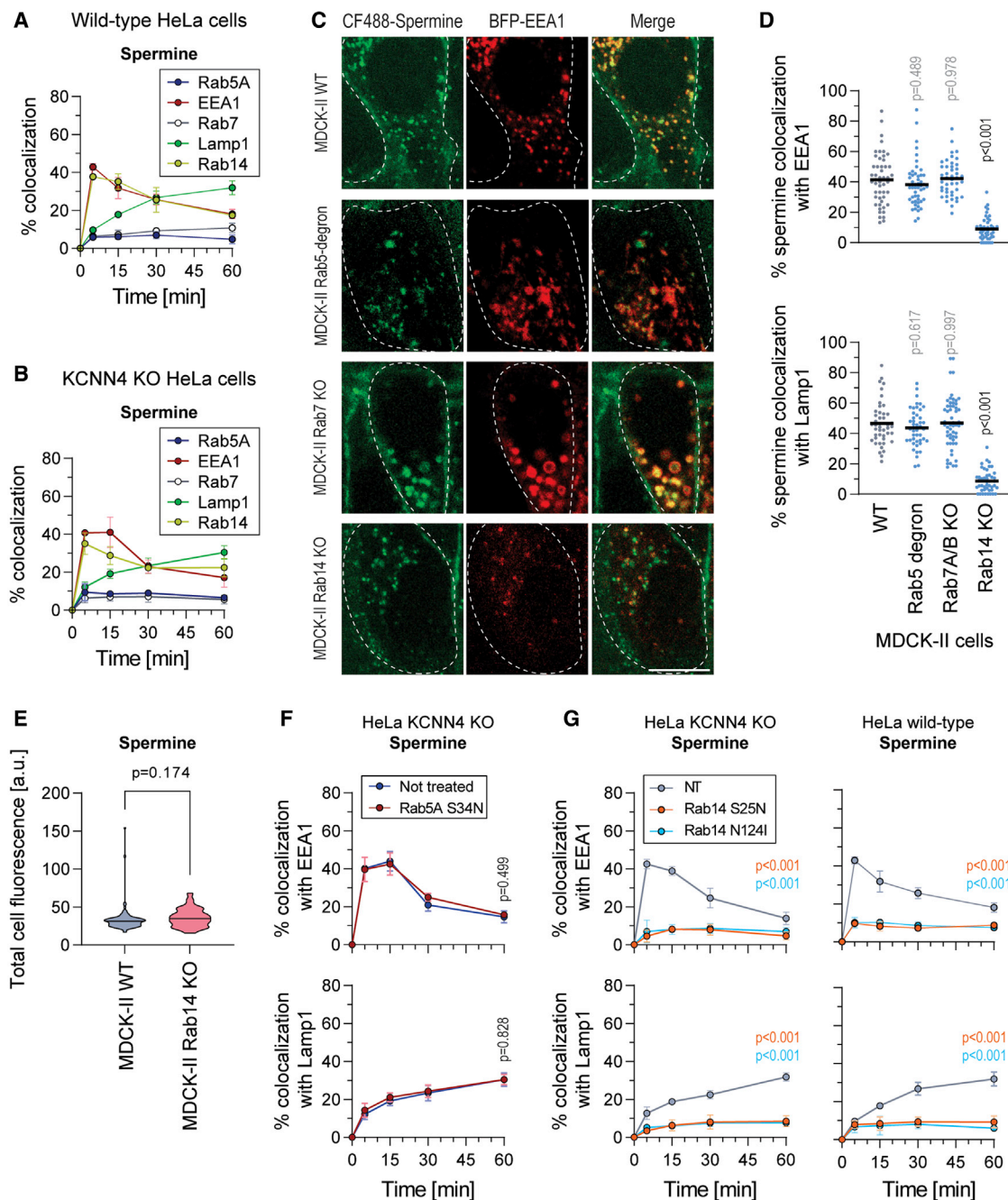


Figure 6. Polyamines are following a Rab5-independent, Rab14-dependent endocytic route

(A and B) Colocalization quantitation between endosomal markers and polyamine. Wild-type (A) and KCNN4 knockout (B) HeLa cells, ectopically expressing RFP-Rab5A, BFP-EEA1, mCherry-Rab7, BFP-LAMP1, or RFP-Rab14, were subjected to a 5 min pulse with fluorescently labeled spermine (5 μ M). Quantitation assessment was based on confocal images. The results correspond to the mean \pm SD of 150–170 analyzed cells per condition derived from three independent experiments.

(C) Representative confocal images of the indicated MDCK-II cell lines ectopically expressing BFP-EEA1, incubated with 5 μ M CF488-spermine for a 5-min pulse. The images correspond to the 15 min time point condition. Scale bar: 10 μ m.

(D) Colocalization quantitation between fluorescent versions of spermine (5 μ M) with BFP-EEA1 (top) or BFP-Lamp1 (bottom) in wild-type and the indicated Rab knockout MDCK-II cells. Cells were incubated for 5 min, then washed and confocal images were acquired at 15 and 30 min post incubation for early and late endosomal markers, respectively. A total of 54–60 cells per condition were analyzed. Statistical analysis was performed with ANOVA multiple comparison to the wild-type condition with Dunett's correction.

(E) Wild-type and Rab14 knockout MDCK-II cells were incubated with 5 μ M CF488-labeled spermine for a 5-min pulse and then analyzed 10 min later. Statistical analysis was done with parametric unpaired t test. A total of 130 cells per condition were analyzed.

(legend continued on next page)

but only marginal colocalization with Rab5A or Rab7A. EEA1 and Lamp1 recruitment to OTX2 HD-positive endosomes was significantly reduced in cells lacking Rab14 (Figures 5C and 5D). The initial OTX2 HD cellular uptake was however not affected (Figure 5E). This indicates that HDs follow a Rab5-independent, Rab14-dependent endosomal maturation pathway.

Polyamines are small signaling molecules involved in several cellular processes (gene regulation, cell proliferation, cell survival, and cell death) (Arruabarrena-Aristorena et al., 2018; Handa et al., 2018; Miller-Fleming et al., 2015; Minois et al., 2011; Ramani et al., 2014). In mammalian cells polyamines enter cells through endocytosis (Soulet et al., 2002; Soulet et al., 2004; Uemura et al., 2010; van Veen et al., 2020), and possibly also through a polyamine specific transporter (Soulet et al., 2004). Polyamine-containing vesicles mature to Lamp1-containing endosomes. At this stage, polyamines are exported to the cytosol (van Veen et al., 2020). The mechanism of polyamines endocytosis has not been described at the molecular level. Similarly to CPPs and HDs, polyamine-containing vesicles colocalized only marginally with Rab5A and Rab7A markers and their maturation down to Lamp1-containing endosomes was Rab14-dependent (Figure 6).

Altogether, these data indicate that physiological molecules such as polyamines, and by extension homeoproteins—if they behave like their homeodomains—do not progress through the classical Rab5-dependent endocytic route but via a Rab14-dependent pathway.

Rab14 is not a specific marker for the CPP endosomal pathway

Before the present work that reports the role of Rab14 in the maturation of CPP-containing endosomes, Rab14 was known to be involved in endosomal recycling (Linford et al., 2012), endosome-endosome fusion, MHC class I cross presentation (Weimershaus et al., 2018) and endosome to Golgi trafficking (Junutula et al., 2004; Proikas-Cezanne et al., 2006). Rab14 has therefore multiple functions and consequently is not likely to reside on a specific set of endosomes. Rab14 colocalizes with the EEA1 and Rab5 early endosomal markers in wild-type and KCNN4 knockout HeLa cells (Figures S7A, S7B, and S7D) (Junutula et al., 2004; Proikas-Cezanne et al., 2006; Ullrich et al., 1996; Yamamoto et al., 2010), but not with late endosomes/lysosomes (Figures S7C–S7E) (Junutula et al., 2004; Proikas-Cezanne et al., 2006; Weimershaus et al., 2018). Rab14 is found as frequently on transferrin-positive vesicles as on CPP-containing endosomes, and to a lesser extent on dextran-positive structures (Figures S7F and S7G) (Junutula et al., 2004). Therefore, while Rab14 is mandatory for the maturation of CPP-containing endosomes, it is not a specific marker for the CPP endocytic pathway.

CPP endosomes mature to Lamp1-positive vesicles that do not correspond to classical lysosomes

To determine if the endosomal pathway taken by CPPs end up in lysosomes with possible degradative functions, we assessed whether the Lamp1-positive, CPP-containing vesicles are acidic. To this end, wild-type and KCNN4 knockout HeLa cells were incubated with LysoSensor Green DND-189, a compound whose fluorescence increases in acidic environment (Figure 7). The majority (~80%) of Lamp1-positive vesicles were acidic but approximately 20% of Lamp1-vesicles were not stained with the LysoSensor dye, regardless of whether the cells were incubated with cargos or not (Figures 7A and 7B). This is in line with published data showing that not all Lamp1-positive compartments are degradative (Cheng et al., 2018; Yap et al., 2018). Unlike dextran-positive endosomes, Lamp1-positive CPP-, OTX2 HD-, or polyamine-containing vesicles were not labeled with the LysoSensor compound (Figures 7C and 7D). These data suggest that CPP-containing vesicles that are positive for Lamp1 are not degradative, further confirming that the CPP endocytic pathway is distinct from Rab5-dependent pathways.

DISCUSSION

We have characterized a previously undescribed Rab5/Rab7-independent, Rab14-dependent endosomal maturation pathway. In this pathway, EEA1 is recruited to early endosomes in the absence of Rab5 (Figures 1, 3, and 4), and endosomal maturation requires Rab14 (Figures 3 and 4). This pathway appears to differ from previously described endocytosis already at the early stages of vesicle formation (Figure 2). We showed that synthetic molecules such as CPPs, as well as physiological molecules such as polyamines take advantage of the Rab5-independent, Rab14-dependent pathway to progress to Lamp1-positive compartments. The endocytosed molecules that we have found to mature via the Rab14-dependent pathway are characterized by their strong cationic nature. Whether this pathway is used by other types of cargos can now be assessed functionally in cells in which Rab14 is inactivated or depleted.

Besides Rab14, no other Rab proteins could be evidenced to play a role in maturation of the endocytic pathway taken by CPPs, HDs, or polyamines. In particular, we did not find a Rab7 homolog that would be required for the acquisition of the Lamp1 marker in this pathway. Rab7 is needed for the maturation to Lamp1-positive acidic vesicles (Lee et al., 2011; Maday et al., 2014; Yap et al., 2018). However, in the Rab14-dependent endocytic maturation pathway, the cargos end up in non-acidic Lamp1-positive vesicles (Figure 7). This indicates that Rab7 controls the acidification of Lamp1-positive endosomes but is not or not always mandatory for endosomal acquisition of Lamp1 as demonstrated by the experiments showing that CPPs do end

(F) Colocalization between spermine with EEA1 (top) or Lamp1 (bottom) in the Rab5A dominant-negative background. HeLa KCNN4 knockout cells expressing the indicated ectopic constructs (GFP-Rab5A S34N, BFP-EEA1, BFP-Lamp1) were incubated for a 5-min pulse with 5 μ M CF647-labeled spermine. The results correspond to the mean \pm SD of three independent experiments. Statistical analysis was performed using parametric two-tailed t test based on AUC values. A total of 150–160 cells per condition were analyzed.

(G) As in (F), except that GFP-Rab14 dominant-negative mutants were used instead of the Rab5 dominant-negative construct. A total of 150–165 cells per condition were analyzed.

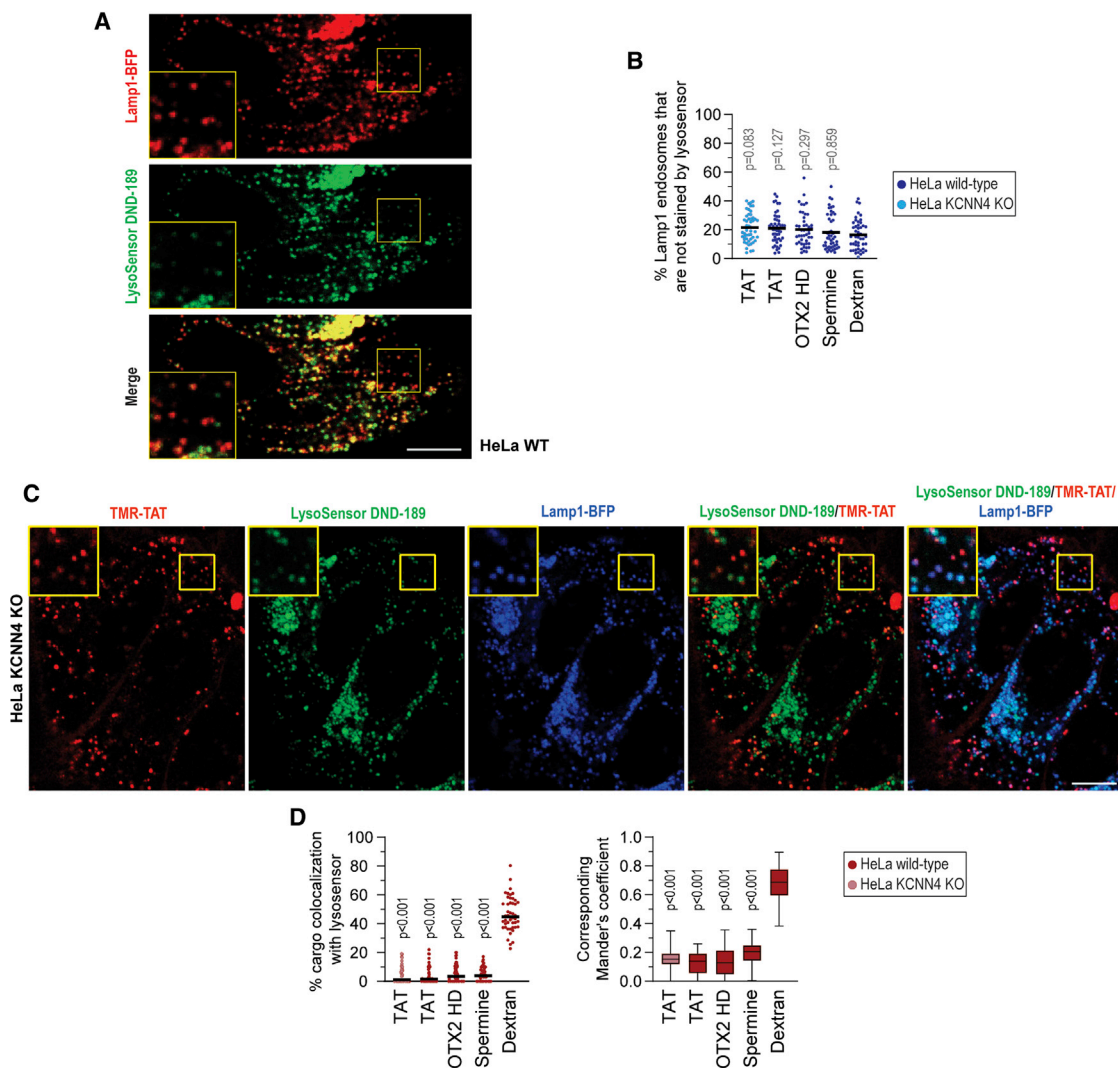


Figure 7. Acidic nature of the CPP- and Lamp1-positive endosomes

(A) Representative confocal images of wild-type HeLa cells expressing Lamp1-BFP incubated for one hour with 1 μ M LysoSensor Green DND-189. Scale bar: 10 μ m.

(B) Colocalization quantitation of acidic Lamp1 vesicles based on confocal images in wild-type and KCNN4 KO HeLa cells incubated with the indicated cargoes for one hour (58 cells per condition were analyzed). Statistical analysis was performed using ANOVA test with Dunnett's correction. The p values correspond to the comparison with dextran. In this graph, all Lamp1-positive vesicles are considered, not only those that colocalize with the indicated markers.

(C) Representative confocal images of KCNN4 knockout HeLa cells expressing Lamp1-BFP incubated for one hour with 40 μ M TMR-TAT and 1 μ M LysoSensor Green DND-189. Scale bar: 10 μ m.

(D) Colocalization quantitation of the indicated endocytic material with lysosensor in wild-type HeLa cells based on visual quantitation (left) or Mander's coefficient (70 cells per condition were analyzed). The cargoes (40 μ M TMR-TAT, 10 μ M OTX2 HD, 5 μ M CF647-labeled spermine, or 0.2 mg/ml TMR-10 kDa dextran) and lysosensor (1 μ M) were incubated with the cells for one hour. Statistical analysis was performed using ANOVA test with Dunnett's correction. The p values correspond to the comparison with cells incubated with dextran.

See also [Figure S7](#).

up in Lamp1-containing compartments in the absence of Rab7 ([Figure 3](#)). The Rab14-dependent endosomal pathway may consequently not require an additional Rab isoform to target its cargoes to Lamp1-positive compartments that are not acidic.

Nonacidic Lamp1-positive cellular compartments have been previously described in the neuronal context ([Cheng et al., 2018](#); [Yap et al., 2018](#)). These vesicles represent the majority of the Lamp1-positive endosomes in neurons ([Cheng et al.,](#)

[2018](#); [Yap et al., 2018](#)). They are Lamp1-positive but negative for Rab7, lysotracker and Cathepsins B and D. The function of such compartments is so far unknown and requires further research. One proposed possibility though is that they correspond to transitory lysosomes ([Cheng et al., 2018](#); [Yap et al., 2018](#)). Such vesicles would originate from maturing endosomes or maturing autophagosomes, which would eventually mature into Lamp1 acidic degradative compartment through retrograde

transport (Cheng et al., 2018; Cheng et al., 2015; Maday et al., 2014; Maday et al., 2012; Yap et al., 2018). Rab7 is thought to be required for the maturation of these nondegradative Lamp1 endosomes into degradative vesicles and subsequent cargo degradation (Lee et al., 2011; Maday et al., 2014; Yap et al., 2018). However, the nonacidic Lamp1-positive vesicles that contain cationic cargos that we have identified in the present work are formed in a Rab7-independent manner and are not acidic. They therefore presumably fulfill nondegradative functions that remain to be investigated.

There was a minimal colocalization between CPP-, HP-, or polyamine-containing endosomes and the Rab5 and Rab7 endosomal markers. This could have resulted from nonselective bulk liquid uptake, as it occurs during macropinocytosis (Palm, 2019). Alternatively, a small fraction of these cargos may specifically enter the Rab5-dependent endosomal pathway as previously reported for some CPPs (Bechara and Sagan, 2013; Futaki et al., 2013; Guidotti et al., 2017; Jones and Sayers, 2012; Koren and Torchilin, 2012; Madani et al., 2011; Trabulo et al., 2010).

There have been earlier circumstantial indications of the existence of a Rab5-independent pathway specifically in the context of viral infections, as well as trafficking to yeast vacuole (Shimamura et al., 2019; Toshima et al., 2014). It has been shown that some viruses use unconventional endocytosis, such as Herpes Simplex Virus 1 (Tebaldi et al., 2020), SARS-CoV (Castaño-Rodríguez et al., 2018), Lassa virus, the Amr53b and We54 strains of LCMV (lymphocytic choriomeningitis virus) (Kunz, 2009; Pasqual et al., 2011; Quirin et al., 2008; Rojek et al., 2008), Lujo virus (Kunz and de la Torre, 2017; Raaben et al., 2017) and some influenza A strains (Wu et al., 2018) that appear to skip the early Rab5-positive endosomes. Rab14 also appears to be involved in viral trafficking, more specifically in the endocytosis of Ebola virus matrix protein VP40 (Fan et al., 2020). Additionally, Rab14 depletion delayed *Candida albicans*-containing phagosome maturation to Lamp1, even though Rab5 and Rab7 markers were still present during the maturation process (Okai et al., 2015). Possibly, the Rab5-independent, Rab14-dependent endosomal pathway is used by some pathogens to infect cells. Therefore, our findings may not only concern the physiological delivery of cationic cargo into cells, but could also be relevant for the search of antiviral or antimicrobial drugs.

Limitations of the study

In the present work we provide evidence for the existence of an endocytic pathway in which both EEA1 recruitment to early endosomes and endosomal maturation to Lamp1-positive endosomes occur in a Rab14-dependent, Rab5/Rab7-independent manner. The mechanism allowing Rab14 to recruit EEA1 on CPP-containing endosomes remains however to be characterized as well as how Rab14, without the apparent need of other Rab proteins, permits the CPP-containing endosomes to mature down to the Lamp1-positive nonacidic compartment. Whether CPPs can escape the endosomes of the Rab14-dependent pathway is not known at the present time. Recent evidence indicate however that the endosomal escape capacity of CPPs is very limited, and it is therefore likely that once cells take up CPPs via the Rab14-dependent pathway, the CPPs do not readily find a way to reach the cytosol (Teo et al., 2021; Trofi-

menko et al., 2021). What also needs to be determined is the physiological relevance of the Rab14 endosomal pathway in the context of polyamine handling by cells or for the signaling properties of homeoproteins.

STAR★METHODS

Detailed methods are provided in the online version of this paper and include the following:

- KEY RESOURCES TABLE
- RESOURCE AVAILABILITY
 - Lead contact
 - Materials availability
 - Data and code availability
- EXPERIMENTAL MODEL AND SUBJECT DETAILS
 - Cell lines
- METHOD DETAILS
 - Reagents
 - Antibodies
 - Western blotting
 - Confocal microscopy
 - Colocalization
 - Immunofluorescence
 - Transient transfection
 - Macropinocytosis inhibition
 - Plasmid constructs
 - Peptides
 - Polyamine labeling
- QUANTIFICATION AND STATISTICAL ANALYSIS

SUPPLEMENTAL INFORMATION

Supplemental information can be found online at <https://doi.org/10.1016/j.celrep.2021.109945>.

ACKNOWLEDGMENTS

This work was supported in part by Grant-in-Aid for Young Scientists from the Ministry of Education, Culture, Sports, Science and Technology (MEXT) of Japan (grant number 20K15739 to Y.H.), Grant-in-Aid for Scientific Research (B) from MEXT (grant number 19H03220 to M.F.), and Japan Science and Technology Agency (JST) CREST (grant number JPMJCR17H4 to M.F.). We are thankful to the Cellular Imaging Facility and Bioinformatics Competence Centre at the University of Lausanne for the resources provided and their technical help.

AUTHOR CONTRIBUTIONS

Conception and design of study, E.T. and C.W.; acquisition of data, E.T.; analysis and/or interpretation of data, E.T., Y.H., M.F., and C.W.; funding acquisition, Y.H., M.F., and C.W.; resources, M.F. and C.W.; drafting the manuscript, E.T. and C.W.; revising the manuscript and approval of the submitted version, all authors.

DECLARATION OF INTERESTS

The authors declare no competing interests.

Received: June 12, 2021
 Revised: August 23, 2021
 Accepted: October 13, 2021
 Published: November 2, 2021

REFERENCES

- Alvarez-Fischer, D., Fuchs, J., Castagner, F., Stettler, O., Massiani-Beaudoin, O., Moya, K.L., Bouillot, C., Oertel, W.H., Lombès, A., Faigle, W., et al. (2011). Engrailed protects mouse midbrain dopaminergic neurons against mitochondrial complex I insults. *Nat. Neurosci.* *14*, 1260–1266.
- Annibaldi, A., Dousse, A., Martin, S., Tazi, J., and Widmann, C. (2011). Revisiting G3BP1 as a RasGAP binding protein: sensitization of tumor cells to chemotherapy by the RasGAP 317-326 sequence does not involve G3BP1. *PLoS ONE*, Published online December 19, 2011. <https://doi.org/10.1371/journal.pone.0029024>.
- Appelbaum, J.S., LaRochelle, J.R., Smith, B.A., Balkin, D.M., Holub, J.M., and Schepartz, A. (2012). Arginine topology controls escape of minimally cationic proteins from early endosomes to the cytoplasm. *Chem. Biol.* *19*, 819–830.
- Araki, N., Hatae, T., Furukawa, A., and Swanson, J.A. (2003). Phosphoinositide-3-kinase-independent contractile activities associated with Fcγ receptor-mediated phagocytosis and macropinocytosis in macrophages. *J. Cell Sci.* *116*, 247–257.
- Arruabarrena-Aristorena, A., Zabala-Letona, A., and Carracedo, A. (2018). Oil for the cancer engine: The cross-talk between oncogenic signaling and polyamine metabolism. *Sci. Adv.* *4*, eaar2606.
- Bain, J., McLaughlan, H., Elliott, M., and Cohen, P. (2003). The specificities of protein kinase inhibitors: an update. *Biochem. J.* *371*, 199–204.
- Balla, A., and Balla, T. (2006). Phosphatidylinositol 4-kinases: old enzymes with emerging functions. *Trends Cell Biol.* *16*, 351–361.
- Barras, D., Lorusso, G., Lhermitte, B., Vierli, D., Rüegg, C., and Widmann, C. (2014a). Fragment N2, a caspase-3-generated RasGAP fragment, inhibits breast cancer metastatic progression. *Int. J. Cancer* *135*, 242–247.
- Barras, D., Lorusso, G., Rüegg, C., and Widmann, C. (2014b). Inhibition of cell migration and invasion mediated by the TAT-RasGAP317-326 peptide requires the DLC1 tumor suppressor. *Oncogene* *33*, 5163–5172.
- Bechara, C., and Sagan, S. (2013). Cell-penetrating peptides: 20 years later, where do we stand? *FEBS Lett.* *587*, 1693–1702.
- Bissig, C., Johnson, S., and Gruenberg, J. (2012). Studying lipids involved in the endosomal pathway. *Methods Cell Biol.* *108*, 19–46.
- Blaudin de Thé, F.X., Rekaik, H., Peze-Heidsieck, E., Massiani-Beaudoin, O., Joshi, R.L., Fuchs, J., and Prochiantz, A. (2018). Engrailed homeoprotein blocks degeneration in adult dopaminergic neurons through LINE-1 repression. *EMBO J.* *37*, e97374.
- Bubb, M.R., Senderowicz, A.M., Sausville, E.A., Duncan, K.L., and Korn, E.D. (1994). Jasplakinolide, a cytotoxic natural product, induces actin polymerization and competitively inhibits the binding of phalloidin to F-actin. *J. Biol. Chem.* *269*, 14869–14871.
- Campa, C.C., Franco, I., and Hirsch, E. (2015). PI3K-C2α: One enzyme for two products coupling vesicle trafficking and signal transduction. *FEBS Lett.* *589*, 1552–1558.
- Castaño-Rodríguez, C., Honrubia, J.M., Gutiérrez-Álvarez, J., DeDiego, M.L., Nieto-Torres, J.L., Jimenez-Guardaño, J.M., Regla-Nava, J.A., Fernandez-Delgado, R., Verdía-Báguena, C., Queralt-Martín, M., et al. (2018). Role of severe acute respiratory syndrome coronavirus viroporins E, 3a, and 8a in replication and pathogenesis. *MBio* *9*, Published online May 22, 2018. <https://doi.org/10.1128/mBio.02325-17>.
- Chaloin, L., Dé, E., Charnet, P., Molle, G., and Heitz, F. (1998). Ionic channels formed by a primary amphipathic peptide containing a signal peptide and a nuclear localization sequence. *Biochim. Biophys. Acta* *1375*, 52–60.
- Chen, Z., and Schmid, S.L. (2020). Evolving models for assembling and shaping clathrin-coated pits. *J. Cell Biol.* *219*, e202005216.
- Cheng, X.T., Zhou, B., Lin, M.Y., Cai, Q., and Sheng, Z.H. (2015). Axonal autophagosomes recruit dynein for retrograde transport through fusion with late endosomes. *J. Cell Biol.* *209*, 377–386.
- Cheng, X.T., Xie, Y.X., Zhou, B., Huang, N., Farfel-Becker, T., and Sheng, Z.H. (2018). Characterization of LAMP1-labeled nondegradative lysosomal and endocytic compartments in neurons. *J. Cell Biol.* *217*, 3127–3139.
- Chevalier, N., Gross, N., and Widmann, C. (2015). Assessment of the chemosensitizing activity of TAT-RasGAP317-326 in childhood cancers. *PLoS ONE* *10*, e0120487.
- Cleal, K., He, L., Watson, P.D., and Jones, A.T. (2013). Endocytosis, intracellular traffic and fate of cell penetrating peptide based conjugates and nanoparticles. *Curr. Pharm. Des.* *19*, 2878–2894.
- Cocucci, E., Aguet, F., Boulant, S., and Kirchhausen, T. (2012). The first five seconds in the life of a clathrin-coated pit. *Cell* *150*, 495–507.
- Deshayes, S., Konate, K., Dussot, M., Chavey, B., Vaissière, A., Van, T.N.N., Aldrian, G., Padari, K., Pooga, M., Vivès, E., et al. (2020). Deciphering the internalization mechanism of WRAP:siRNA nanoparticles. *Biochim. Biophys. Acta Biomembr.* *1862*, 183252.
- Dharmawardhane, S., Schürmann, A., Sells, M.A., Chernoff, J., Schmid, S.L., and Bokoch, G.M. (2000). Regulation of macropinocytosis by p21-activated kinase-1. *Mol. Biol. Cell* *11*, 3341–3352.
- Di Nardo, A.A., Fuchs, J., Joshi, R.L., Moya, K.L., and Prochiantz, A. (2018). The Physiology of Homeoprotein Transduction. *Physiol. Rev.* *98*, 1943–1982.
- Dinneen, J.L., and Ceresa, B.P. (2004). Expression of dominant negative rab5 in HeLa cells regulates endocytic trafficking distal from the plasma membrane. *Exp. Cell Res.* *294*, 509–522.
- Duchardt, F., Fotin-Mleczek, M., Schwarz, H., Fischer, R., and Brock, R. (2007). A comprehensive model for the cellular uptake of cationic cell-penetrating peptides. *Traffic* *8*, 848–866.
- Fan, J., Liu, X., Mao, F., Yue, X., Lee, I., and Xu, Y. (2020). Proximity proteomics identifies novel function of Rab14 in trafficking of Ebola virus matrix protein VP40. *Biochem. Biophys. Res. Commun.* *527*, 387–392.
- Fili, N., Calleja, V., Woscholski, R., Parker, P.J., and Larjani, B. (2006). Compartmental signal modulation: Endosomal phosphatidylinositol 3-phosphate controls endosome morphology and selective cargo sorting. *Proc. Natl. Acad. Sci. USA* *103*, 15473–15478.
- Fujimoto, L.M., Roth, R., Heuser, J.E., and Schmid, S.L. (2000). Actin assembly plays a variable, but not obligatory role in receptor-mediated endocytosis in mammalian cells. *Traffic* *1*, 161–171.
- Futaki, S., and Nakase, I. (2017). Cell-Surface Interactions on Arginine-Rich Cell-Penetrating Peptides Allow for Multiplex Modes of Internalization. *Acc. Chem. Res.* *50*, 2449–2456.
- Futaki, S., Hirose, H., and Nakase, I. (2013). Arginine-rich peptides: methods of translocation through biological membranes. *Curr. Pharm. Des.* *19*, 2863–2868.
- Gautreau, A., Oguievetskaia, K., and Ungermann, C. (2014). Function and regulation of the endosomal fusion and fission machineries. *Cold Spring Harb. Perspect. Biol.* *6*, 24591520. Published online March 5, 2014. <https://doi.org/10.1101/cshperspect.a016832>.
- Gozzelino, L., De Santis, M.C., Gulluni, F., Hirsch, E., and Martini, M. (2020). PI(3,4)P2 signaling in cancer and metabolism. *Front. Oncol.* *10*, 360.
- Guidotti, G., Brambilla, L., and Rossi, D. (2017). Cell-penetrating peptides: From basic research to clinics. *Trends Pharmacol. Sci.* *38*, 406–424.
- Handa, A.K., Fatima, T., and Mattoo, A.K. (2018). Polyamines: Bio-molecules with diverse functions in plant and human health and disease. *Front. Chem.* *6*, 10.
- Hasegawa, J., Tokuda, E., Tenno, T., Tsujita, K., Sawai, H., Hiroaki, H., Takenawa, T., and Itoh, T. (2011). SH3YL1 regulates dorsal ruffle formation by a novel phosphoinositide-binding domain. *J. Cell Biol.* *193*, 901–916.
- Heulot, M., Chevalier, N., Puyal, J., Margue, C., Michel, S., Kreis, S., Kulms, D., Barras, D., Nahimana, A., and Widmann, C. (2016). The TAT-RasGAP317-326 anti-cancer peptide can kill in a caspase-, apoptosis-, and necroptosis-independent manner. *Oncotarget* *7*, 64342–64359.
- Heulot, M., Jacquier, N., Aeby, S., Le Roy, D., Roger, T., Trofimenko, E., Baras, D., Greub, G., and Widmann, C. (2017). The anticancer peptide TAT-RasGAP317-326 exerts broad antimicrobial activity. *Front. Microbiol.* *8*, 994.
- Homma, Y., Kinoshita, R., Kuchitsu, Y., Wawro, P.S., Marubashi, S., Oguchi, M.E., Ishida, M., Fujita, N., and Fukuda, M. (2019). Comprehensive knockout

- analysis of the Rab family GTPases in epithelial cells. *J. Cell Biol.* **218**, 2035–2050.
- Huotari, J., and Helenius, A. (2011). Endosome maturation. *EMBO J.* **30**, 3481–3500.
- Illien, F., Rodriguez, N., Amoura, M., Joliot, A., Pallerla, M., Cribier, S., Burlina, F., and Sagan, S. (2016). Quantitative fluorescence spectroscopy and flow cytometry analyses of cell-penetrating peptides internalization pathways: Optimization, pitfalls, comparison with mass spectrometry quantification. *Sci. Rep.* **6**, 36938.
- Jaber, N., Mohd-Naim, N., Wang, Z., DeLeon, J.L., Kim, S., Zhong, H., Sheshadri, N., Dou, Z., Edinger, A.L., Du, G., et al. (2016). Vps34 regulates Rab7 and late endocytic trafficking through recruitment of the GTPase-activating protein Armus. *J. Cell Sci.* **129**, 4424–4435.
- Johannes, L., Parton, R.G., Bassereau, P., and Mayor, S. (2015). Building endocytic pits without clathrin. *Nat. Rev. Mol. Cell Biol.* **16**, 311–321.
- Johns, H.L., Berryman, S., Monaghan, P., Belsham, G.J., and Jackson, T. (2009). A dominant-negative mutant of rab5 inhibits infection of cells by foot-and-mouth disease virus: implications for virus entry. *J. Virol.* **83**, 6247–6256.
- Jones, A.T., and Sayers, E.J. (2012). Cell entry of cell penetrating peptides: tales of tails wagging dogs. *J. Control. Release* **167**, 582–591.
- Jordan, M., Schallhorn, A., and Wurm, F.M. (1996). Transfecting mammalian cells: optimization of critical parameters affecting calcium-phosphate precipitate formation. *Nucleic Acids Res.* **24**, 596–601.
- Junutula, J.R., De Mazière, A.M., Peden, A.A., Ervin, K.E., Advani, R.J., van Dijk, S.M., Klumperman, J., and Scheller, R.H. (2004). Rab14 is involved in membrane trafficking between the Golgi complex and endosomes. *Mol. Biol. Cell* **15**, 2218–2229.
- Kaksonen, M., and Roux, A. (2018). Mechanisms of clathrin-mediated endocytosis. *Nat. Rev. Mol. Cell Biol.* **19**, 313–326.
- Kaplan, I.M., Wadia, J.S., and Dowdy, S.F. (2005). Cationic TAT peptide transduction domain enters cells by macropinocytosis. *J. Control. Release* **102**, 247–253.
- Kawaguchi, Y., Takeuchi, T., Kuwata, K., Chiba, J., Hatanaka, Y., Nakase, I., and Futaki, S. (2016). Syndecan-4 Is a Receptor for Clathrin-Mediated Endocytosis of Arginine-Rich Cell-Penetrating Peptides. *Bioconjug. Chem.* **27**, 1119–1130.
- Koivusalo, M., Welch, C., Hayashi, H., Scott, C.C., Kim, M., Alexander, T., Touret, N., Hahn, K.M., and Grinstein, S. (2010). Amiloride inhibits macropinocytosis by lowering submembranous pH and preventing Rac1 and Cdc42 signaling. *J. Cell Biol.* **188**, 547–563.
- Koren, E., and Torchilin, V.P. (2012). Cell-penetrating peptides: breaking through to the other side. *Trends Mol. Med.* **18**, 385–393.
- Kristensen, M., Birch, D., and Mørck Nielsen, H. (2016). Applications and Challenges for Use of Cell-Penetrating Peptides as Delivery Vectors for Peptide and Protein Cargos. *Int. J. Mol. Sci.* **17**, Published online January 30, 2016. <https://doi.org/10.3390/ijms17020185>.
- Kunz, S. (2009). Receptor binding and cell entry of Old World arenaviruses reveal novel aspects of virus-host interaction. *Virology* **387**, 245–249.
- Kunz, S., and de la Torre, J.C. (2017). Breaking the barrier: Host cell invasion by Lujo virus. *Cell Host Microbe* **22**, 583–585.
- Langemeyer, L., Fröhlich, F., and Ungermann, C. (2018). Rab GTPase function in endosome and lysosome biogenesis. *Trends Cell Biol.* **28**, 957–970.
- Lee, S., Sato, Y., and Nixon, R.A. (2011). Lysosomal proteolysis inhibition selectively disrupts axonal transport of degradative organelles and causes an Alzheimer's-like axonal dystrophy. *J. Neurosci.* **31**, 7817–7830.
- Linford, A., Yoshimura, S., Nunes Bastos, R., Langemeyer, L., Gerondopoulos, A., Rigden, D.J., and Barr, F.A. (2012). Rab14 and its exchange factor FAM116 link endocytic recycling and adherens junction stability in migrating cells. *Dev. Cell* **22**, 952–966.
- Madani, F., Lindberg, S., Langel, U., Futaki, S., and Gräslund, A. (2011). Mechanisms of cellular uptake of cell-penetrating peptides. *J. Biophys.* **2011**, 414729.
- Maday, S., Wallace, K.E., and Holzbaur, E.L. (2012). Autophagosomes initiate distally and mature during transport toward the cell soma in primary neurons. *J. Cell Biol.* **196**, 407–417.
- Maday, S., Twelvetrees, A.E., Moughamian, A.J., and Holzbaur, E.L. (2014). Axonal transport: cargo-specific mechanisms of motility and regulation. *Neuron* **84**, 292–309.
- Maekawa, M., Terasaka, S., Mochizuki, Y., Kawai, K., Ikeda, Y., Araki, N., Skolnik, E.Y., Taguchi, T., and Arai, H. (2014). Sequential breakdown of 3-phosphorylated phosphoinositides is essential for the completion of macropinocytosis. *Proc. Natl. Acad. Sci. USA* **111**, E978–E987.
- McBride, H.M., Rybin, V., Murphy, C., Giner, A., Teasdale, R., and Zerial, M. (1999). Oligomeric complexes link Rab5 effectors with NSF and drive membrane fusion via interactions between EEA1 and syntaxin 13. *Cell* **98**, 377–386.
- Mercer, J., Schelhaas, M., and Helenius, A. (2010). Virus entry by endocytosis. *Annu. Rev. Biochem.* **79**, 803–833.
- Miaczynska, M., and Zerial, M. (2002). Mosaic organization of the endocytic pathway. *Exp. Cell Res.* **272**, 8–14.
- Michod, D., Yang, J.Y., Chen, J., Bonny, C., and Widmann, C. (2004). A Ras-GAP-derived cell permeable peptide potently enhances genotoxin-induced cytotoxicity in tumor cells. *Oncogene* **23**, 8971–8978.
- Michod, D., Annibaldi, A., Schaefer, S., Dapples, C., Rochat, B., and Widmann, C. (2009). Effect of RasGAP N2 fragment-derived peptide on tumor growth in mice. *J. Natl. Cancer Inst.* **101**, 828–832.
- Miller-Fleming, L., Olin-Sandoval, V., Campbell, K., and Ralsler, M. (2015). Remaining mysteries of molecular biology: The role of polyamines in the cell. *J. Mol. Biol.* **427**, 3389–3406.
- Mills, I.G., Jones, A.T., and Clague, M.J. (1998). Involvement of the endosomal autoantigen EEA1 in homotypic fusion of early endosomes. *Curr. Biol.* **8**, 881–884.
- Minois, N., Carmona-Gutierrez, D., and Madeo, F. (2011). Polyamines in aging and disease. *Aging (Albany NY)* **3**, 716–732.
- Mrozowska, P.S., and Fukuda, M. (2016). Regulation of podocalyxin trafficking by Rab small GTPases in 2D and 3D epithelial cell cultures. *J. Cell Biol.* **213**, 355–369.
- Mueller, J., Kretzschmar, I., Volkmer, R., and Boisguerin, P. (2008). Comparison of cellular uptake using 22 CPPs in 4 different cell lines. *Bioconjug. Chem.* **19**, 2363–2374.
- Murray, D.H., Jahnel, M., Lauer, J., Avellaneda, M.J., Brouilly, N., Cezanne, A., Morales-Navarrete, H., Perini, E.D., Ferguson, C., Lupas, A.N., et al. (2016). An endosomal tether undergoes an entropic collapse to bring vesicles together. *Nature* **537**, 107–111.
- Naguib, A. (2016). Following the trail of lipids: Signals initiated by PI3K function at multiple cellular membranes. *Sci. Signal.* **9**, re4.
- Nakase, I., Niwa, M., Takeuchi, T., Sonomura, K., Kawabata, N., Koike, Y., Takehashi, M., Tanaka, S., Ueda, K., Simpson, J.C., et al. (2004). Cellular uptake of arginine-rich peptides: roles for macropinocytosis and actin rearrangement. *Mol. Ther.* **10**, 1011–1022.
- Naslavsky, N., and Caplan, S. (2018). The enigmatic endosome - sorting the ins and outs of endocytic trafficking. *J. Cell Sci.* **131**, Published on July 6, 2018. <https://doi.org/10.1242/jcs.216499>.
- Nishimura, K., Fukagawa, T., Takisawa, H., Kakimoto, T., and Kanemaki, M. (2009). An auxin-based degron system for the rapid depletion of proteins in nonplant cells. *Nat. Methods* **6**, 917–922.
- Okai, B., Lyall, N., Gow, N.A., Bain, J.M., and Erwig, L.P. (2015). Rab14 regulates maturation of macrophage phagosomes containing the fungal pathogen *Candida albicans* and outcome of the host-pathogen interaction. *Infect. Immun.* **83**, 1523–1535.
- Palm, W. (2019). Metabolic functions of macropinocytosis. *Philos. Trans. R. Soc. Lond. B Biol. Sci.* **374**, 20180285.
- Pasqual, G., Rojek, J.M., Masin, M., Chatton, J.Y., and Kunz, S. (2011). Old world arenaviruses enter the host cell via the multivesicular body and depend

- on the endosomal sorting complex required for transport. *PLoS Pathog.* **7**, e1002232.
- Pittet, O., Petermann, D., Michod, D., Krueger, T., Cheng, C., Ris, H.B., and Widmann, C. (2007). Effect of the TAT-RasGAP(317-326) peptide on apoptosis of human malignant mesothelioma cells and fibroblasts exposed to meso-tetra-hydroxyphenyl-chlorin and light. *J. Photochem. Photobiol. B* **88**, 29–35.
- Polyakov, V., Sharma, V., Dahlheimer, J.L., Pica, C.M., Luker, G.D., and Piwnicka-Worms, D. (2000). Novel Tat-peptide chelates for direct transduction of technetium-99m and rhenium into human cells for imaging and radiotherapy. *Bioconjug. Chem.* **11**, 762–771.
- Posor, Y., Eichhorn-Gruenig, M., Puchkov, D., Schöneberg, J., Ullrich, A., Lampe, A., Müller, R., Zarbakhsh, S., Gulluni, F., Hirsch, E., et al. (2013). Spatiotemporal control of endocytosis by phosphatidylinositol-3,4-bisphosphate. *Nature* **499**, 233–237.
- Prochiantz, A., and Di Nardo, A.A. (2015). Homeoprotein signaling in the developing and adult nervous system. *Neuron* **85**, 911–925.
- Proikas-Cezanne, T., Gaugel, A., Frickey, T., and Nordheim, A. (2006). Rab14 is part of the early endosomal clathrin-coated TGN microdomain. *FEBS Lett.* **580**, 5241–5246.
- Quirin, K., Eschli, B., Scheu, I., Poort, L., Kartenbeck, J., and Helenius, A. (2008). Lymphocytic choriomeningitis virus uses a novel endocytic pathway for infectious entry via late endosomes. *Virology* **378**, 21–33.
- Raaben, M., Jae, L.T., Herbert, A.S., Kuehne, A.I., Stubbs, S.H., Chou, Y.Y., Blomen, V.A., Kirchhausen, T., Dye, J.M., Brummelkamp, T.R., and Whelan, S.P. (2017). NRP2 and CD63 are host factors for Lujo virus cell entry. *Cell Host Microbe* **22**, 688–696.e5.
- Räägel, H., Säälk, P., and Pooga, M. (2010). Peptide-mediated protein delivery-which pathways are penetrable? *Biochim. Biophys. Acta* **1798**, 2240–2248.
- Ramadani, F., Bolland, D.J., Garcon, F., Emery, J.L., Vanhaesebroeck, B., Corcoran, A.E., and Okkenhaug, K. (2010). The PI3K isoforms p110alpha and p110delta are essential for pre-B cell receptor signaling and B cell development. *Sci. Signal.* **3**, ra60.
- Ramani, D., De Bandt, J.P., and Cynober, L. (2014). Aliphatic polyamines in physiology and diseases. *Clin. Nutr.* **33**, 14–22.
- Rekaik, H., Blaudin de Thé, F.X., Fuchs, J., Massiani-Beaudoin, O., Prochiantz, A., and Joshi, R.L. (2015a). Engrailed homeoprotein protects mesencephalic dopaminergic neurons from oxidative stress. *Cell Rep.* **13**, 242–250.
- Rekaik, H., Blaudin de Thé, F.X., Prochiantz, A., Fuchs, J., and Joshi, R.L. (2015b). Dissecting the role of Engrailed in adult dopaminergic neurons—Insights into Parkinson disease pathogenesis. *FEBS Lett.* **26459030** Published online October 13, 2015. <https://doi.org/10.1016/j.febslet.2015.10.002>.
- Rojek, J.M., Perez, M., and Kunz, S. (2008). Cellular entry of lymphocytic choriomeningitis virus. *J. Virol.* **82**, 1505–1517.
- Rothbard, J.B., Jessop, T.C., Lewis, R.S., Murray, B.A., and Wender, P.A. (2004). Role of membrane potential and hydrogen bonding in the mechanism of translocation of guanidinium-rich peptides into cells. *J. Am. Chem. Soc.* **126**, 9506–9507.
- Ruseska, I., and Zimmer, A. (2020). Internalization mechanisms of cell-penetrating peptides. *Beilstein J. Nanotechnol.* **11**, 101–123.
- Sagan, S., Burlina, F., Alves, I.D., Bechara, C., Dupont, E., and Joliot, A. (2013). Homeoproteins and homeoprotein-derived peptides: going in and out. *Curr. Pharm. Des.* **19**, 2851–2862.
- Sampath, P., and Pollard, T.D. (1991). Effects of cytochalasin, phalloidin, and pH on the elongation of actin filaments. *Biochemistry* **30**, 1973–1980.
- Santos, M.de.S., Naal, R.M., Baird, B., and Holowka, D. (2013). Inhibitors of PI(4,5)P2 synthesis reveal dynamic regulation of IgE receptor signaling by phosphoinositides in RBL mast cells. *Mol. Pharmacol.* **83**, 793–804.
- Schmid, S.L., Sorkin, A., and Zerial, M. (2014). Endocytosis: Past, present, and future. *Cold Spring Harb. Perspect. Biol.* **6**, a022509.
- Schneider, C.A., Rasband, W.S., and Eliceiri, K.W. (2012). NIH Image to ImageJ: 25 years of image analysis. *Nat. Methods* **9**, 671–675.
- Scott, C.C., Vacca, F., and Gruenberg, J. (2014). Endosome maturation, transport and functions. *Semin. Cell Dev. Biol.* **31**, 2–10.
- Serulla, M., Ichim, G., Stojceski, F., Grasso, G., Afonin, S., Heulot, M., Schober, T., Roth, R., Godefroy, C., Milhiet, P.E., et al. (2020). TAT-RasGAP₃₁₇₋₃₂₆ kills cells by targeting inner-leaflet-enriched phospholipids. *Proc. Natl. Acad. Sci. USA* **117**, 31871–31881.
- Shimamura, H., Nagano, M., Nakajima, K., Toshima, J.Y., and Toshima, J. (2019). Rab5-independent activation and function of yeast Rab7-like protein, Ypt7p, in the AP-3 pathway. *PLoS ONE* **14**, e0210223.
- Sieczkarski, S.B., and Whittaker, G.R. (2003). Differential requirements of Rab5 and Rab7 for endocytosis of influenza and other enveloped viruses. *Traffic* **4**, 333–343.
- Simonsen, A., Lippé, R., Christoforidis, S., Gaullier, J.M., Brech, A., Callaghan, J., Toh, B.H., Murphy, C., Zerial, M., and Stenmark, H. (1998). EEA1 links PI(3)K function to Rab5 regulation of endosome fusion. *Nature* **394**, 494–498.
- Soulet, D., Covassin, L., Kaouass, M., Charest-Gaudreault, R., Audette, M., and Poulin, R. (2002). Role of endocytosis in the internalization of spermidine-C(2)-BODIPY, a highly fluorescent probe of polyamine transport. *Biochem. J.* **367**, 347–357.
- Soulet, D., Gagnon, B., Rivest, S., Audette, M., and Poulin, R. (2004). A fluorescent probe of polyamine transport accumulates into intracellular acidic vesicles via a two-step mechanism. *J. Biol. Chem.* **279**, 49355–49366.
- Spatazza, J., Di Lullo, E., Joliot, A., Dupont, E., Moya, K.L., and Prochiantz, A. (2013). Homeoprotein signaling in development, health, and disease: a shaking of dogmas offers challenges and promises from bench to bed. *Pharmacol. Rev.* **65**, 90–104.
- Sugiyama, S., Di Nardo, A.A., Aizawa, S., Matsuo, I., Volovitch, M., Prochiantz, A., and Hensch, T.K. (2008). Experience-dependent transfer of Otx2 homeoprotein into the visual cortex activates postnatal plasticity. *Cell* **134**, 508–520.
- Takei, K., and Haucke, V. (2001). Clathrin-mediated endocytosis: membrane factors pull the trigger. *Trends Cell Biol.* **11**, 385–391.
- Tebaldi, G., Pritchard, S.M., and Nicola, A.V. (2020). Herpes simplex virus entry by a nonconventional endocytic pathway. *J. Virol.* **94**, Published on November 23, 2021. <https://doi.org/10.1128/JVI.01910-20>.
- Teo, S.L.Y., RENNICK, J.J., Yuen, D., Al-Wassiti, H., Jpublished ohnston, A.P.R., and Pouton, C.W. (2021). Unravelling cytosolic delivery of cell penetrating peptides with a quantitative endosomal escape assay. *Nat. Commun.* **12**, 3721.
- Thottacherry, J.J., Sathe, M., Prabhakara, C., and Mayor, S. (2019). Spoiled for choice: Diverse endocytic pathways function at the cell surface. *Annu. Rev. Cell Dev. Biol.* **35**, 55–84.
- Torero Ibad, R., Rhee, J., Mrejen, S., Forster, V., Picaud, S., Prochiantz, A., and Moya, K.L. (2011). Otx2 promotes the survival of damaged adult retinal ganglion cells and protects against excitotoxic loss of visual acuity in vivo. *J. Neurosci.* **31**, 5495–5503.
- Torriani, G., Trofimenko, E., Mayor, J., Fedeli, C., Moreno, H., Michel, S., Heulot, M., Chevalier, N., Zimmer, G., Shrestha, N., et al. (2019). Identification of clotrimazole-derivatives as specific inhibitors of Arenavirus fusion. *J. Virol.* **93**, Published on March 5, 2019. <https://doi.org/10.1128/JVI.01744-18>.
- Toshima, J.Y., Nishinoaki, S., Sato, Y., Yamamoto, W., Furukawa, D., Siekhaus, D.E., Sawaguchi, A., and Toshima, J. (2014). Bifurcation of the endocytic pathway into Rab5-dependent and -independent transport to the vacuole. *Nat. Commun.* **5**, 3498.
- Trabulo, S., Cardoso, A.L., Mano, M., and De Lima, M.C. (2010). Cell-Penetrating Peptides-Mechanisms of Cellular Uptake and Generation of Delivery Systems. *Pharmaceuticals (Basel)* **3**, 961–993.
- Trofimenko, E., Grasso, G., Heulot, M., Chevalier, N., Deriu, M.A., Dubuis, G., Arribat, Y., Serulla, M., Michel, S., Vantomme, G., et al. (2021). Genetic, cellular and structural characterization of the membrane potential-dependent cell-penetrating peptide translocation pore. *BioRxiv*. <https://doi.org/10.1101/2020.02.25.963017>.
- Tsoutsou, P., Annibaldi, A., Viertel, D., Ollivier, J., Buchegger, F., Vozenin, M.C., Bourhis, J., Widmann, C., and Matzinger, O. (2017). TAT-RasGAP₃₁₇₋₃₂₆

Enhances Radiosensitivity of Human Carcinoma Cell Lines In Vitro and In Vivo through Promotion of Delayed Mitotic Cell Death. *Radiat. Res.* **187**, 562–569.

Uemura, T., Stringer, D.E., Blohm-Mangone, K.A., and Gerner, E.W. (2010). Polyamine transport is mediated by both endocytic and solute carrier transport mechanisms in the gastrointestinal tract. *Am. J. Physiol. Gastrointest. Liver Physiol.* **299**, G517–G522.

Ullrich, O., Reinsch, S., Urbé, S., Zerial, M., and Parton, R.G. (1996). Rab11 regulates recycling through the pericentriolar recycling endosome. *J. Cell Biol.* **135**, 913–924.

van Veen, S., Martin, S., Van den Haute, C., Benoy, V., Lyons, J., Vanhoutte, R., Kahler, J.P., Decuypere, J.P., Gelders, G., Lambie, E., et al. (2020). ATP13A2 deficiency disrupts lysosomal polyamine export. *Nature* **578**, 419–424.

Vasconcelos, L., Pärn, K., and Langel, U. (2013). Therapeutic potential of cell-penetrating peptides. *Ther. Deliv.* **4**, 573–591.

Viaud, J., and Peterson, J.R. (2009). An allosteric kinase inhibitor binds the p21-activated kinase autoregulatory domain covalently. *Mol. Cancer Ther.* **8**, 2559–2565.

Wadia, J.S., Stan, R.V., and Dowdy, S.F. (2004). Transducible TAT-HA fusogenic peptide enhances escape of TAT-fusion proteins after lipid raft macropinocytosis. *Nat. Med.* **10**, 310–315.

Wallbrecher, R., Ackels, T., Olea, R.A., Klein, M.J., Caillon, L., Schiller, J., Bo-vée-Geurts, P.H., van Kuppevelt, T.H., Ulrich, A.S., Spehr, M., et al. (2017). Membrane permeation of arginine-rich cell-penetrating peptides independent of transmembrane potential as a function of lipid composition and membrane fluidity. *J. Control. Release* **256**, 68–78.

Weimershaus, M., Mauvais, F.X., Saveanu, L., Adiko, C., Babdor, J., Abramova, A., Montealegre, S., Lawand, M., Evnouchidou, I., Huber, K.J., et al.

(2018). Innate Immune Signals Induce Anterograde Endosome Transport Promoting MHC Class I Cross-Presentation. *Cell Rep.* **24**, 3568–3581.

Wenk, M.R., and De Camilli, P. (2004). Protein-lipid interactions and phosphoinositide metabolism in membrane traffic: insights from vesicle recycling in nerve terminals. *Proc. Natl. Acad. Sci. USA* **101**, 8262–8269.

Wu, Q.M., Liu, S.L., Chen, G., Zhang, W., Sun, E.Z., Xiao, G.F., Zhang, Z.L., and Pang, D.W. (2018). Uncovering the Rab5-independent autophagic trafficking of influenza A virus by quantum-dot-based single-virus tracking. *Small* **14**, e1702841.

Xie, J., Bi, Y., Zhang, H., Dong, S., Teng, L., Lee, R.J., and Yang, Z. (2020). Cell-penetrating peptides in diagnosis and treatment of human diseases: From pre-clinical research to clinical application. *Front. Pharmacol.* **11**, 697.

Yamamoto, H., Koga, H., Katoh, Y., Takahashi, S., Nakayama, K., and Shin, H.W. (2010). Functional cross-talk between Rab14 and Rab4 through a dual effector, RUFY1/Rabip4. *Mol. Biol. Cell* **21**, 2746–2755.

Yap, C.C., Digilio, L., McMahon, L.P., Garcia, A.D.R., and Winckler, B. (2018). Degradation of dendritic cargos requires Rab7-dependent transport to somatic lysosomes. *J. Cell Biol.* **217**, 3141–3159.

Zeigerer, A., Gilleron, J., Bogorad, R.L., Marsico, G., Nonaka, H., Seifert, S., Epstein-Barash, H., Kuchimanchi, S., Peng, C.G., Ruda, V.M., et al. (2012). Rab5 is necessary for the biogenesis of the endolysosomal system in vivo. *Nature* **485**, 465–470.

Zhang, X., Jin, Y., Plummer, M.R., Pooyan, S., Gunaseelan, S., and Sinko, P.J. (2009). Endocytosis and membrane potential are required for HeLa cell uptake of R.I.-CKTat9, a retro-inverso Tat cell penetrating peptide. *Mol. Pharm.* **6**, 836–848.

Zhang, S.X., Duan, L.H., He, S.J., Zhuang, G.F., and Yu, X. (2017). Phosphatidylinositol 3,4-bisphosphate regulates neurite initiation and dendrite morphogenesis via actin aggregation. *Cell Res.* **27**, 253–273.

STAR★METHODS

KEY RESOURCES TABLE

REAGENT or RESOURCE	SOURCE	IDENTIFIER
Antibodies		
Mouse monoclonal anti-EEA1	BD Transduction Laboratories	RRID:AB_397830
Mouse monoclonal anti-Lamp1	BD PharMingen	RRID:AB_396132
Rabbit polyclonal phospho-AKT (Ser473)	Cell signaling	Cat# 92715
Anti-Rab5C antiserum	Mitsunori Fukuda laboratory; <i>J Cell Biol</i> 213 , 355-369 (2016)	N/A
Donkey polyclonal anti-mouse Cy3 secondary antibody	Jackson ImmunoResearch	RRID:AB_2340813
Chemicals, Peptides, and Recombinant Proteins		
Hoechst 3342	Thermo Fisher	Cat# H21492
AlexaFluor488-Transferrin	Thermo Fisher	Cat# T13342
AlexaFluor568-Transferrin	Thermo Fisher	Cat# T23365
AlexaFluor647-Transferrin	Thermo Fisher	Cat# T23366
TMR-Dextran 10'000	Thermo Fisher	Cat# D1816
AlexaFluor647-EGF	Thermo Fisher	Cat# E35351
EIPA	Stephan Kunz laboratory, Sigma Aldrich	Cat# A3085
IPA3	Stephan Kunz laboratory, Sigma Aldrich	Cat# I2285
ML7	Stephan Kunz laboratory, Sigma Aldrich	Cat# I2764
CytoD	Stephan Kunz laboratory, Sigma Aldrich	Cat# C8273
Jas	Stephan Kunz laboratory, Sigma Aldrich	Cat# J4580
LY294002	Sigma Aldrich	Cat# 440202
Wortmannin	Sigma Aldrich	Cat# W1344
Indole-3-acetic acid	Sigma-Aldrich	Cat# I2886
Doxycycline	Sigma-Aldrich	Cat# D3447
Lipofectamin 2000	Thermo Fisher	Cat# 11668030
Fluoromount-G	cBioscience	Cat# 00-4958-02
Restriction enzyme: BamHI	New England Biolabs	Cat# R313614
Restriction enzyme: BspEI	New England Biolabs	Cat# R0540S
TMR- and FITC-TAT-RasGAP317-326	SBS Genetech	N/A
TMR- or FITC-TAT	SBS Genetech	N/A
TMR- or FITC-R9	SBS Genetech	N/A
TMR- or FITC -Penetratin	SBS Genetech	N/A
TMR- or FITC -MAP	SBS Genetech	N/A
TMR- or FITC -Transportan	SBS Genetech	N/A
FITC-OTX2 HD	SBS Genetech	N/A
Critical Commercial Assays		
Mix-n-Stain Small Ligand Labeling Kit CF405M	Biotium	Cat# 92362
Mix-n-Stain Small Ligand Labeling Kit CF594	Biotium	Cat# 92352
Q5® Site-Directed Mutagenesis Kit	New England Biolabs	Cat# E0554S
Deposited Data		
Image randomizer script	This paper	https://github.com/BICC-UNIL-EPFL/randomizer

(Continued on next page)

REAGENT or RESOURCE	SOURCE	IDENTIFIER
Continued		
Experimental Models: Cell Lines		
Dog: MDCK-II parental and Rab knockout cell lines	RIKEN BioResource Research Center Cell Bank	Cat#: RCB5099–RCB5148
Dog: MDCK-II Rab5 knockout and degran-Rab5A-expressing cell line	Mitsunori Fukuda laboratory (Homma et al., manuscript in preparation)	N/A
Human: HeLa	ATCC	CCL-2
Oligonucleotides		
Primer: introducing dominant negative mutations in GFP-hRab5B(S34N). Forward: AGTGGGAAAGaacAGCCTGGTATTAC	This paper	N/A
Primer: introducing dominant negative mutations in GFP-hRab5B(S34N). Reverse: GCAGATTCTCCAGCAGG	This paper	N/A
Primer: introducing dominant negative mutations in GFP-hRab22(S19N). Forward: TGTAGGTAAaacAGTATTGTGGCGG	This paper	N/A
Primer: introducing dominant negative mutations in GFP-hRab22(S19N). Reverse: CCTGTATCCCGAGCAGA	This paper	N/A
Recombinant DNA		
Plasmid: RFP-hRab5A.dn3	Addgene	Cat# 14437
Plasmid: mCh-hRab7A	Addgene	Cat# 61804
Plasmid: GFP-hRab5A.dn3	Stephan Kunz laboratory	Pasqual et al., 2011
Plasmid: GFP-hRab7A.dn3	Stephan Kunz laboratory	Pasqual et al., 2011
Plasmid: GFP-DynI.dn3	Stephan Kunz laboratory	Pasqual et al., 2011
Plasmid: GFP-hRab5A(S34N).dn3	Stephan Kunz laboratory	Pasqual et al., 2011
Plasmid: GFP-Rab7A(T22N).dn3	Stephan Kunz laboratory	Pasqual et al., 2011
Plasmid: GFP-DynI(K44A).dn3	Stephan Kunz laboratory	Pasqual et al., 2011
Plasmid: mCh-hRab5A(S34N)	Addgene	Cat# 35139
Plasmid: GFP-hRab5B.dn3	Addgene	Cat# 61802
Plasmid: GFP-hRab5B(S34N)	This paper	
Plasmid: GFP-Rab5C.dn3	Genescript	Cat# OHu09753C
Plasmid: CFP-hRab5C(S35N).dn3	Addgene	Cat# 11504
Plasmid: GFP-hEEA1	Addgene	Cat# 42307
Plasmid: hLamp1-GFP.dn3	Addgene	Cat# 34831
Plasmid: BFP-hRab7A-Myc	Addgene	Cat# 79803
Plasmid: hLamp1-BFP	Addgene	Cat# 98828
Plasmid: GFP-hRab14.dn3	Addgene	Cat# 49549
Plasmid: GFP-hRab14(S25N).dn3	Addgene	Cat# 49594
Plasmid: GFP-hRab14(N124I).dn3	Addgene	Cat# 49593
Software and Algorithms		
ImageJ	Schneider et al., 2012	https://imagej.nih.gov/ij/
Zeiss Zen Lite 2.3	Carl Zeiss Microscopy GmbH	https://www.zeiss.fr/microscopie/produits/microscope-software/zen-lite.html
GraphPad Prism8	GraphPad	https://www.graphpad.com/scientific-software/prism/
Clone Manager9	Sci-Ed Software	https://www.scied.com/dl_cm10.htm
Li-Cor Odyssey	LI-COR Biosciences	N/A
Image randomizer	This paper	Zenodo: https://doi.org/10.5281/zenodo.5553413

RESOURCE AVAILABILITY

Lead contact

Further information and requests for resources and reagents should be directed to and will be fulfilled by the Lead Contact, Christian Widmann (christian.widmann@unil.ch).

Materials availability

This study did not generate new unique reagents.

Data and code availability

- All data reported in this paper will be shared by the lead contact upon request.
- All original code has been deposited at Zenodo and is publicly available as of the date of publication. DOIs are listed in the key resources table.
- Any additional information required to reanalyze the data reported in this paper is available from the Lead Contact upon request.

EXPERIMENTAL MODEL AND SUBJECT DETAILS

Cell lines

All cell lines were cultured in 5% CO₂ at 37°C. HeLa (ATCC: CCL-2) cells were cultured in RPMI media (61870044; Thermo Fisher,) supplemented with 10% heat-inactivated fetal bovine serum (FBS; 10270-106; Thermo Fisher). MDCK-II parental and knock-out cell lines⁹⁹ (available from RIKEN BioResource Research Center Cell Bank (RCB5099–RCB5148; <https://cell.brc.riken.jp/en>) were cultured in DMEM (10566016; Thermo Fisher), 10% FBS. MDCK-II Rab5 knock-out and degran-Rab5A-expressing cell line will be described elsewhere (Homma et al., manuscript in preparation).

METHOD DETAILS

Reagents

Live Hoechst 33342 (CDS023389, Sigma) was aliquoted and stored at –20°C. AlexaFluor488-, AlexaFluor568-, AlexaFluor647-labeled human transferrin was dissolved in PBS at 5 mg/ml and stored at 4°C (T13342, T23365 and T23366; Thermo Fisher). TMR-labeled 10,000 neutral dextran was dissolved in PBS at 10 mg/ml and stored at –20°C (D1816; Thermo Fisher). AlexaFluor647-labeled and biotinylated epidermal growth factor (EGF) was dissolved in water at 1 mg/ml, aliquoted and stored at –20°C (E35351; Thermo Fisher). EIPA (stock concentration 10 mM), IPA3 (stock concentration 5 mM), ML7 (stock concentration 10 mM), CytoD (stock concentration 1 mM), Jas (stock concentration 1 mM) a kind gift from Stefan Kunz laboratory, were dissolved in DMSO, aliquoted and stored at –20°C. LY294002 was dissolved in DMSO at 20 mg/ml, aliquoted and stored at –20°C (440202; Sigma Aldrich). Wortmannin was aliquoted in DMSO at a 50 mg/ml concentration and stored at –20°C (W1628; Sigma Aldrich). Indole-3-acetic acid (IAA) (I2886; Sigma-Aldrich) was dissolved in ethanol at a 500 mM concentration, aliquoted and stored at –20°C. Doxycycline (D3447; Sigma-Aldrich) was dissolved in DMSO at a 1 mg/ml concentration, aliquoted and stored at –20°C. LysoTracker Red DND-99 (L7528; Thermo Fisher) and LysoSensor Green DND-189 (L7535; Thermo Fisher) were stored at a 1 mM concentration at –20°C.

Antibodies

The mouse monoclonal anti-EEA1, stored at –20°C (610457; BD Transduction Laboratories) and anti-Lamp1, stored at 4°C (555798; BD PharMingen) antibodies were used in immunofluorescence experiments. Donkey polyclonal anti-mouse Cy3 secondary antibody was aliquoted and stored at –20°C in glycerol (715-165-150; Jackson ImmunoResearch). Phospho-AKT (Ser473) rabbit polyclonal antibody was stored at –20°C (92715; Cell signaling) and was used for western blotting. Anti-Rab5C antiserum, which can recognize all three Rab5 isoforms (Mrozowska and Fukuda, 2016), was stored at –20°C.

Western blotting

Cells were lysed in the NP-40 lysis buffer. Protein concentrations in the cell lysates were quantitated by Bradford assay and 20 µg protein per sample were loaded onto 10% polyacrylamide gel. After the transfer, the nitrocellulose membranes were stained with 0.1% Ponceau S solution. The membrane was incubated with the indicated primary antibodies for 16 hours at 4°C, washed three times for 20 minutes in PBS-tween 0.1%, incubated with a secondary antibody for 1 hour at room temperature and washed three times for 20 minutes in PBS-Tween 0.1%. Detection was done with Odyssey infrared imaging system (LICOR Biosciences, Bad Homburg, Germany).

Confocal microscopy

Confocal microscopy experiments were done on live cells. Cells were seeded onto glass bottom culture dishes (P35G-1.5-14-C; MatTek, corporation) and treated as described in the figures. For pulse-chase experiments, cells were incubated with the indicated cargos for 5 minutes at 37°C in 5% CO₂. Cells were then washed twice with media on ice and imaged immediately after. These images correspond to the 5-minute time point in the figures. Additional images were acquired at 15-, 30- and 60-minute post cargo addition. Approximately 10 different random regions within the sample dish were sampled per time point. In between these acquisition times, the cells were placed in 37°C, 5% CO₂ incubator. For nuclear staining, 10 µg/ml live Hoechst 33342 (H21492; Molecular probes) was added in the culture medium 5 minutes before washing cells twice with media. Image acquisition was performed with a plan Apochromat 63x oil immersion objective mounted on a Zeiss LSM 780 laser scanning fluorescence confocal microscope equipped with gallium arsenide phosphide detectors and three lasers (a 405 nm diode laser, a 458-476-488-514 nm argon laser, and a 561 nm diode-pumped solid-state laser). Acquisition was done in “smart setup” mode that allows the acquisition with simultaneous excitation and detection of several fluorophores. This allows the selected probes to be recorded with minimum delay. Image resolution was 0.10 µm x 0.10 µm per pixel and pinhole size was set to maximum 1 AU or below (0.5 AU in the case of Figure 1D). We checked that there was no leakage of a given fluorophore signal into the other fluorophore emission channels when multi-fluorophore recordings were done. Cell images were acquired at a focal plane near the middle of the cell making sure that nuclei were visible. Experiments at 20°C were done using an incubation chamber set at 20°C, 5% CO₂ and visualized with a Zeiss LSM710 Quasar laser scanning fluorescence confocal microscope equipped with Neofluar 63x, 1.2 numerical aperture (NA) and using the same lasers and settings as above. Image resolution with Zeiss LSM710 microscope was 0.13 µm x 0.13 µm per pixel. In colocalization experiments, when the cargos are labeled with fluorophores emitting in the red spectrum, the endosomal markers are either labeled with GFP or BFP. When the cargos are labeled with fluorophores emitting in the green spectrum, the endosomal markers are either labeled with RFP, mCherry, or BFP.

Colocalization

Colocalization assessment between endocytosed material and a given endosomal marker was performed on confocal images by visual assessment, switching back and forth between the color channels (Figure S1B). Only fully overlapping signals were considered belonging to the same endosomes while partially colocalized signals were not considered being derived from the same vesicles but rather assumed to originate from closely positioned particles that are artifactually overlapping due to insufficient resolution and excess fluorophore intensities. The samples were randomized to blind the experimentators from the nature of the samples they were analyzing. The randomization script is available at Zenodo: <https://doi.org/10.5281/zenodo.5553413>. The visual quantitation was validated by Mander's and Pearson's coefficient calculation performed on the same samples using the JaCoP plugin in ImageJ. Examples of colocalization quantitation analysis is shown in Figures S1B and S1C.

Immunofluorescence

Immunofluorescence experiments for the localization of endogenous and ectopically expressed EEA1 and Lamp1 endosomal markers (Figure S2A-B) was performed as described (Bissig et al., 2012). Briefly, cells were plated on poly L-lysine-coated coverslips and fixed with 4% paraformaldehyde for 20 minutes at room temperature at the indicated time points after treatment. Following a 5-minute permeabilization at room temperature in PBS, 0.25% Triton X-100, the samples were blocked for 20 minutes at room temperature in PBS, 3% BSA. Incubation with primary antibodies was done for two hours at room temperature in PBS, 1% BSA. The cells were then incubated for 45 minutes at room temperature with Cy3-labeled secondary antibodies in the same buffers as above. Coverslips were finally incubated 5 minutes with PBS, 10 µg/ml Hoechst 33342. Three PBS washes were done between each incubation steps. Coverslips were mounted in Fluoromount-G (00-4958-02; cBioscience). Samples were visualized with a Zeiss LSM780 confocal microscope.

Transient transfection

Calcium-phosphate-based transfection of HeLa cells was performed as previously described (Jordan et al., 1996). Briefly, cells were plated overnight in DMEM (61965; Invitrogen) medium supplemented with 10% heat-inactivated FBS (10270-106; Invitrogen), 2.5 µg of total plasmid DNA of interest was diluted in water, CaCl₂ was added to the DNA and the mixture was incubated with an equal volume of HEPES 2x for 60 s before adding the mixture drop by drop to the cells. Media was changed 10 hours later.

Transient transfection in MDCK cells was done with Lipofectamin 2000 reagent according to supplier's instructions with 2.5 µg of total plasmid DNA (11668030; Thermo Fisher).

Macropinocytosis inhibition

Cells ectopically expressing GFP-EEA1 were starved overnight to stimulate macropinocytosis. Media was then changed to RPMI containing 10% FBS and cells were preincubated for 30 minutes with the indicated macropinocytosis inhibitors (kind gift from Dr. Stephan Kunz lab). Cells were pulsed for 5 minutes with TMR-dextran or TMR-TAT-RasGAP₃₁₇₋₃₂₆, washed and visualized under confocal microscope in RPMI, 10% FBS in the presence of macropinocytosis inhibitors.

Plasmid constructs

The RFP-hRab5A.dn3 (#921) plasmid encoding RFP-labeled human Rab5A protein was from Addgene (Cat# 14437). The mCh-hRab7A (#922) plasmid encoding mCherry-labeled human Rab7A protein was from Addgene (Cat# 61804). GFP-hRab5A.dn3 (#966), GFP-hRab7A.dn3 (#968), GFP-Dynl.dn3 (#963) plasmids encoding GFP-labeled versions of the indicated human proteins, as well as their dominant-negative isoforms [plasmids GFP-hRab5A(S34N).dn3 (#961), GFP-Rab7A(T22N).dn3 (#969), GFP-Dynl(-K44A).dn3 (#964)] were a kind gift from Stefan Kunz laboratory. The mCh-hRab5(S34N) (#933) plasmid encoding a mCherry-labeled dominant-negative mutant version of human Rab5A was from Addgene (Cat# 35139). The GFP-hRab5B.dn3 (#1008) plasmid encoding GFP-labeled wild-type version of human Rab5B isoform was from Addgene (Cat# 61802). The GFP-hRab5B(S34N) (#1067) plasmid encoding GFP-labeled dominant negative mutant version of human Rab5B isoform was introduced to plasmid GFP-hRab5B.dn3 (#1008) using Q5 Site-Directed Mutagenesis kit (NEB, Cat# E0554S) according to manufacturer's instructions using forward primer #1554 (AGTGGGAAAGaacAGCCTGGTATTAC; the lower-case letters are those that introduce the mutation creating the dominant-negative version of the protein) and reverse primer #1555 (GCAGATTCTCCCAGCAGG). The GFP-Rab5C.dn3 (#1074) plasmid encoding GFP-labeled version of human Rab5C isoform was from Genescript (Cat# OHu09753C). GFP-hRab5C(S35N).dn3 (#1006) encoding cerulean-labeled dominant-negative mutant version of human Rab5C isoform was from Addgene (Cat# 11504). GFP-hEEA1 (#970) and hLamp1-GFP.dn3 (#971) encoding GFP-labeled versions of human EEA1 and Lamp1, respectively were from Addgene (Cat# 42307 and 34831). The BFP-EEA1 (#1009) plasmid was generated by subcloning the EEA1 portion of GFP-hEEA1 (#970) into BFP-hRab7A-Myc (#1005, Addgene Cat# 79803) from which the hRab7-Myc fragment was removed. This was achieved by digestion of both plasmids with BamHI (NEB, Cat# R313614) and BspEI (NEB, Cat# R0540S) and ligation of the EEA1 insert into the vector fragment lacking hRab7-Myc. The hLamp1-BFP (#1016) plasmid encoding BFP-labeled version of human Lamp1 protein was from Addgene (Cat# 98828). The GFP-hRab14.dn3 (#1017) plasmid encoding GFP-labeled human Rab14 was from Addgene (Cat# 49549). The GFP-hRab14(S25N).dn3 (#1037) and GFP-hRab14(N124I).dn3 (#1038) plasmids encoding GFP-labeled versions of dominant-negative Rab14 mutant were from Addgene (Cat# 49594 and 49593).

Peptides

TAT-RasGAP₃₁₇₋₃₂₆ is a retro-inverso peptide (i.e., synthesized with D-amino-acids in the opposite direction compared to the natural sequence) labeled or not with FITC or TMR. The TAT moiety corresponds to amino acids 48–57 of the HIV TAT protein (RRRQRRKRG) and the RasGAP₃₁₇₋₃₂₆ moiety corresponds to amino acids from 317 to 326 of the human RasGAP protein (DTRLNTVMMW). These two moieties are separated by two glycine linker residues in the TAT-Ras-GAP₃₁₇₋₃₂₆ peptide. The following CPPs, TAT, MAP (KLALKLALK ALKAALKLA), Penetratin (RQIKWFQRRMKWKK), Transportan (GWTLSAGYLLGKINLKALAALAKKIL), R9 (RRRRRRRRR), were synthesized in the retro-inverso conformation (and also in the natural L-amino acid conformation in the case of TAT). They were labeled with either FITC or TMR at the N terminus. The sequence of the OTX2 HD (QRRERTTFTR AQLDVLEALF AKTRYPDIFM REEVALKINL PESRVQWFK NRRRAKCRQQQ) was synthesized with L-amino acids and was labeled with FITC or TMR at the N terminus. All peptides were synthesized by SBS Genetech, China and resuspended to 1 mM in water.

Polyamine labeling

Spermine fluorescent labeling with CF405M, CF488A, CF647, and CF594 dyes was performed using a Mix-n-Stain Small Ligand Labeling Kit (92362, 92350, 92359, and 92352, respectively; Biotium) according to manufacturer's instructions.

QUANTIFICATION AND STATISTICAL ANALYSIS

Statistical analysis was performed on non-normalized data, using GraphPad Prism 7. All measurements were from biological replicates. Unless otherwise stated, the vertical bars in the graph represent the standard deviation of mean from at least three independent experiments. The details of statistical tests applied for the analysis, the exact number of cells analyzed per condition, can be found in the figure legends.

Cell Reports, Volume 37

Supplemental information

**The endocytic pathway taken by cationic
substances requires Rab14 but not Rab5 and Rab7**

Evgeniya Trofimenko, Yuta Homma, Mitsunori Fukuda, and Christian Widmann

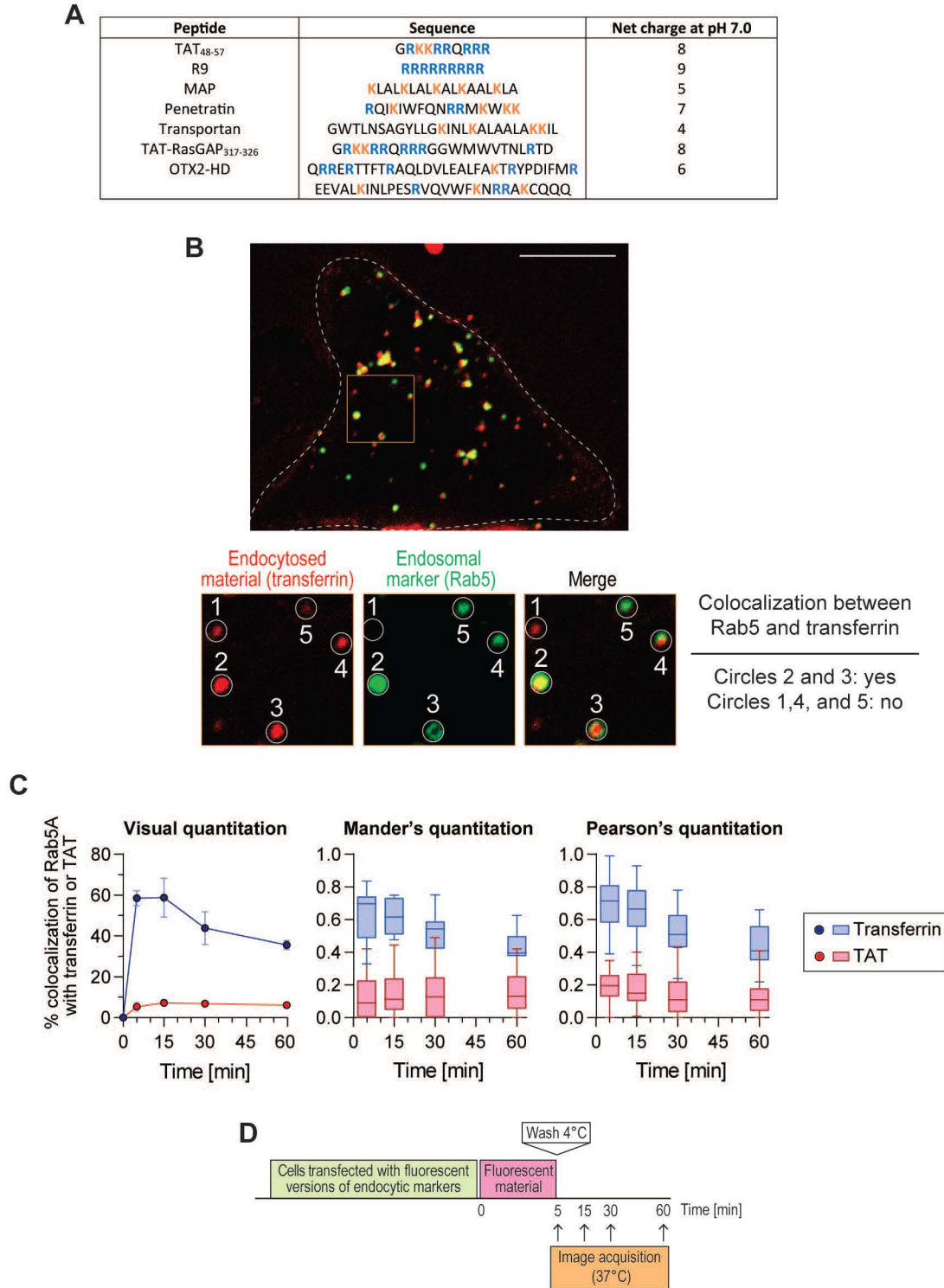


Figure S1. Colocalization quantitation and experimental setup. Related to Figure 1.

(A) CPP sequences and the net charge they carry. Positively charged amino acids (arginine and lysine) are color-coded.

(B) Visual assessment of the colocalization between fluorescently labeled endosomal material and endocytic markers. Samples were randomized to blind the experimenters from the nature of the samples they were analyzing. Colocalization assessment was performed visually by switching back and forth between the color channels. The image at the top shows a representative confocal image of one KCNN4 knock-out HeLa cell expressing GFP-Rab5A incubated with 20 μ g/ml AlexaFluor568-transferrin for 5 minutes. The bottom images are enlarged regions of the cell shown above. They depict how we determined whether colocalization between Rab5 and transferrin occurred or not. For example, the red and green signals in circle 4 do not have overlapping centers and are therefore not considered to belong to the same vesicle. In contrast, the red and green signals in circles 2 and 3 have overlapping centers and are consequently considered to belong to the same vesicles. Scale bar: 10 μ m.

(C) KCNN4 knock-out HeLa cells expressing GFP-Rab5A were incubated with 20 μ g/ml AlexaFluor568-Transferrin or 40 μ M TMR-TAT for 5 minutes. Colocalization between Rab5A and either transferrin or TAT was quantitated visually as described in panel B (mean \pm SD of 156-165 cells per condition derived from three independent experiments). Alternatively, colocalization was assessed by Mander's or Pearson's quantitation using the JaCoP plugin in ImageJ (shown as box plots) on the same cells used for the visual quantitation.

(D) Unless otherwise mentioned, the time-course experiments performed in the present work follow the setting presented in this panel. Cells expressing fluorescent versions of endocytic markers are incubated five minutes with various fluorescent material, washed, and the endosomal maturation followed overtime.

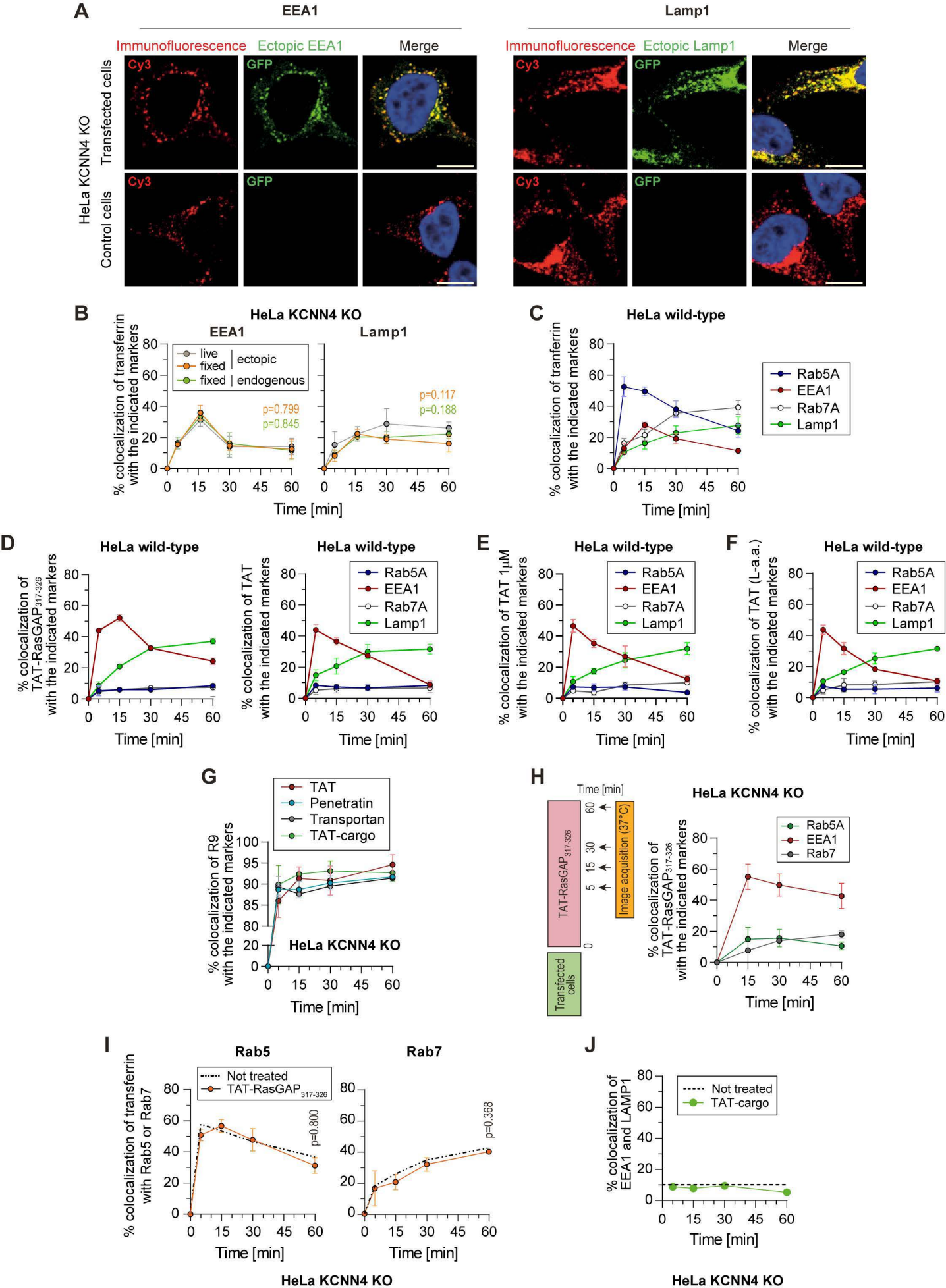


Figure S2. Experimental setup controls. Related to Figure 1.

(A) Ectopic expression does not alter the subcellular location of endosomal markers. KCNN4 knock-out HeLa cells were transfected (top row) or not (bottom row) with GFP-tagged versions of EEA1 and Lamp1. EEA1 and Lamp1 were visualized in fixed cells by immunofluorescence (Cy3 signal) or via GFP fluorescence. Scale bar: 10 μm .

(B) Quantitation of the colocalization between ectopic GFP-tagged or endogenous EEA1 or Lamp1 with Alexa568-transferrin in live or fixed KCNN4 knock-out HeLa cells. Cells were treated as depicted in Figure S1D and then either fixed and immunostained with anti-EEA1 or anti-Lamp1 antibodies or visualized live by confocal microscopy. The data correspond to the mean \pm SD of 160-171 cells per condition derived from three independent experiments. The p-values were calculated using ANOVA analysis with Dunett's correction based on area under the curve (AUC) values. Green p values: live cells expressing ectopic markers vs fixed control cells. Orange p values: live cells expressing ectopic markers vs fixed cells expressing ectopic markers.

(C) Quantitation of colocalization between transferrin (20 $\mu\text{g/ml}$) and fluorescently-tagged early and late endosomal markers in wild-type HeLa cells. The data correspond to the mean \pm SD of 160-171 cells per condition derived from three independent experiments.

(D) Quantitation of colocalization between TAT-RasGAP₃₁₇₋₃₂₆ or TAT (both used at a 40 μM concentration) and fluorescently-tagged early and late endosomal markers in HeLa wild-type cells. The data correspond to the mean \pm SD of 150-160 cells per condition derived from three independent experiments.

(E) Quantitation of colocalization between TAT (1 μM) and fluorescently-tagged early and late endosomal markers in wild-type HeLa cells. The data correspond to the mean \pm SD of 150-160 cells per condition derived from three independent experiments.

(F) Quantitation of colocalization between TAT (40 μM) with natural L-amino acid conformation and fluorescently-tagged early and late endosomal markers in wild-type HeLa cells. The data correspond to the mean \pm SD of 150-160 cells per condition derived from three independent experiments.

(G) Colocalization quantitation of the indicated FITC-labelled CPPs with TMR-R9 in KCNN4 knock-out HeLa cells. The data correspond to the mean \pm SD of 170-181 cells per condition derived from three independent experiments.

(H) Colocalization between TAT-RasGAP₃₁₇₋₃₂₆ (40 μM) and GFP-tagged Rab5, EEA1 or Rab7 in KCNN4 knock-out HeLa cells. Cells were incubated in the continuous presence of TAT-RasGAP₃₁₇₋₃₂₆ as indicated on the left-hand side of the panel. The data correspond to the mean \pm SD of 150-165 cells per condition derived from three independent experiments.

(I) Colocalization in KCNN4 knock-out HeLa cells between transferrin and Rab5 (top) or Rab7 (bottom) in the presence (TAT-cargo) or in the absence (not treated) of 40 μM TAT-RasGAP₃₁₇₋₃₂₆. The data correspond to the mean \pm SD of 165-170 cells per condition derived from three independent experiments. The p-values were calculated on AUC values using parametric two-tailed unpaired t-tests.

(J) Colocalization quantitation in KCNN4 knock-out HeLa cells between ectopically expressed BFP-EEA1 and Lamp1-GFP in the presence (TAT-cargo) or in the absence (not treated) of 40 μM TAT-RasGAP₃₁₇₋₃₂₆. The data correspond to the mean \pm SD of 165-178 cells per condition derived from three independent experiments.

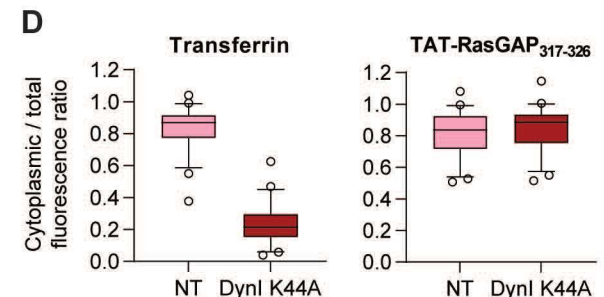
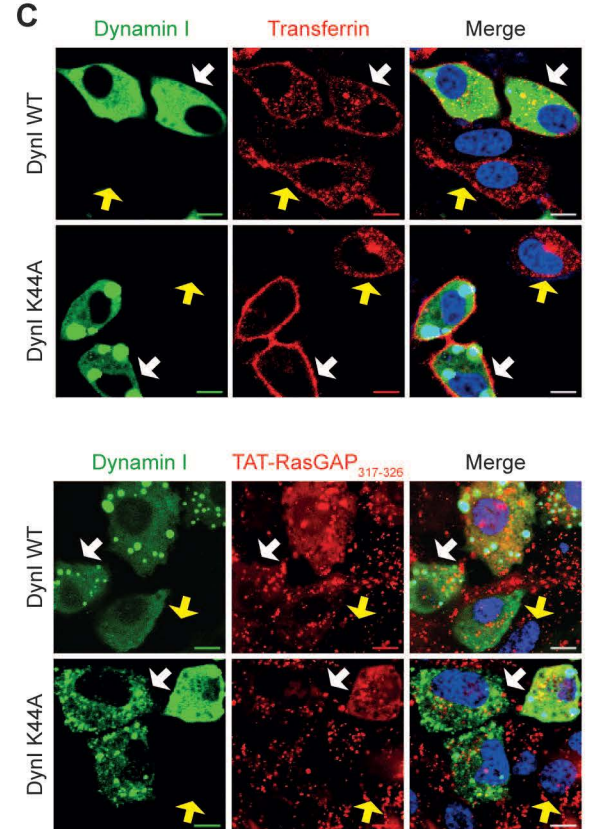
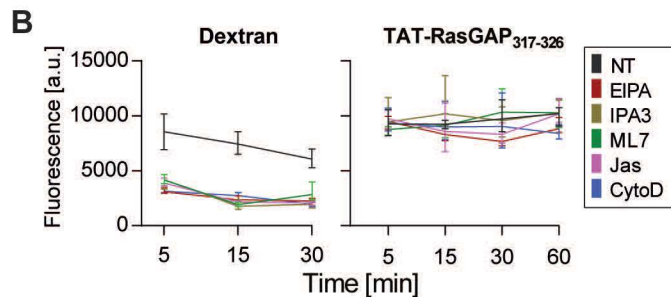
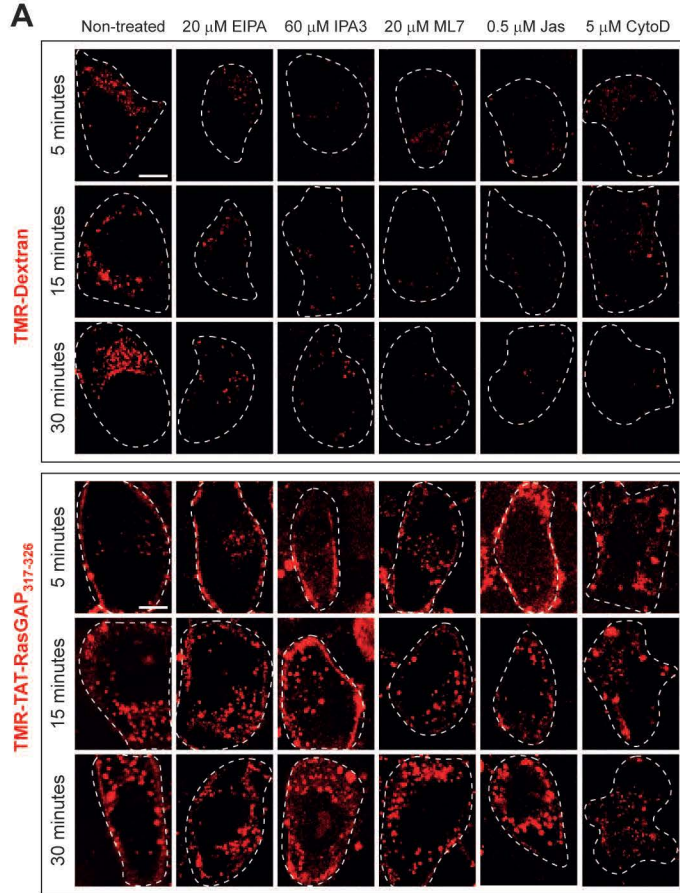


Figure S3. Macropinosome formation inhibitors and dynamin dominant-negative mutants do not affect CPP uptake. Related to Figure 1.

(A) Representative confocal images of KCNN4 knock-out HeLa cells preincubated or not with the indicated inhibitors for 30 minutes prior to the addition of 0.2 mg/ml TMR 10 kDa Dextran or 40 μ M TMR-TAT-RasGAP₃₁₇₋₃₂₆ for a 5-minute pulse. Confocal images were acquired at 5, 30 and 60 minutes after the addition of the cargoes. The inhibitors were present throughout the full duration of the experiment. Scale bar: 10 μ m.

(B) Total cell fluorescence quantitation based on images acquired in panel A. Results correspond to the mean \pm SD of 150-168 cells per condition derived from three independent experiments.

(C) Representative confocal images of KCNN4 knock-out HeLa cells ectopically expressing wild-type (Dynl WT) or dominant-negative (Dynl K44A) version of dynamin I. Cells were incubated with 20 μ g/ml AlexaFluor568-transferrin or 40 μ M TMR-TAT-RasGAP₃₁₇₋₃₂₆. Cell nuclei were labeled with live Hoechst. White arrows point to cells transfected with GFP-dynamin constructs and yellow arrows indicate non-transfected cells. Images were acquired at 15 minutes post incubation with the cargoes. Scale bar: 10 μ m.

(D) Cytosolic/total fluorescence ratio based on confocal images acquired in panel C. Cytosolic/total fluorescence ratio corresponds to the proportion of transferrin or TMR-TAT-RasGAP₃₁₇₋₃₂₆ fluorescence signal found within the cell's cytosol normalized to total cell fluorescence (minus the signal found in the nucleus that was excluded based on Hoechst staining). A low cytosolic ratio indicates that the signal mostly originates from the cell membrane. Calculations were done using ImageJ. A total of 150 cells per condition were analyzed derived from three independent experiments.

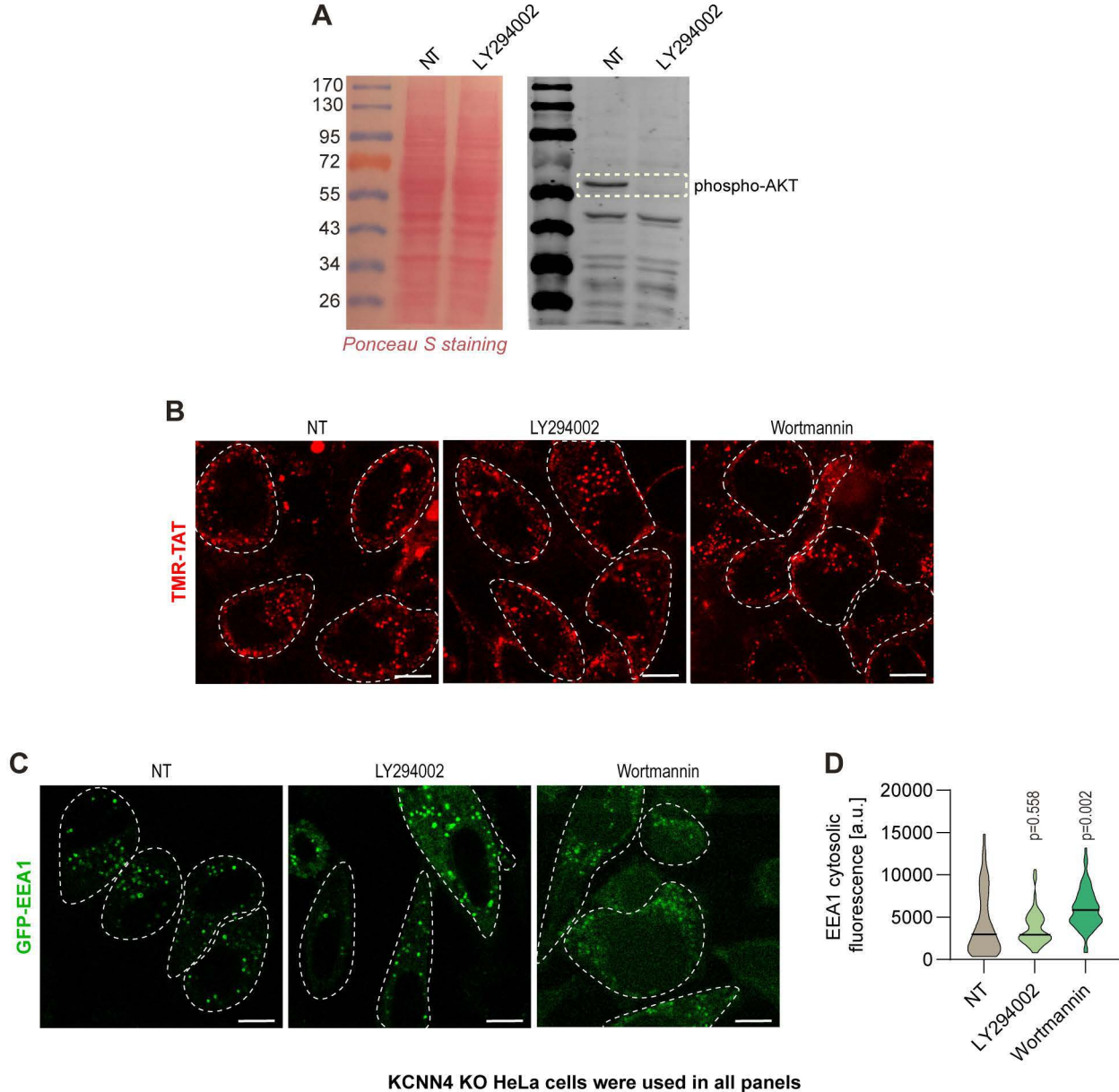


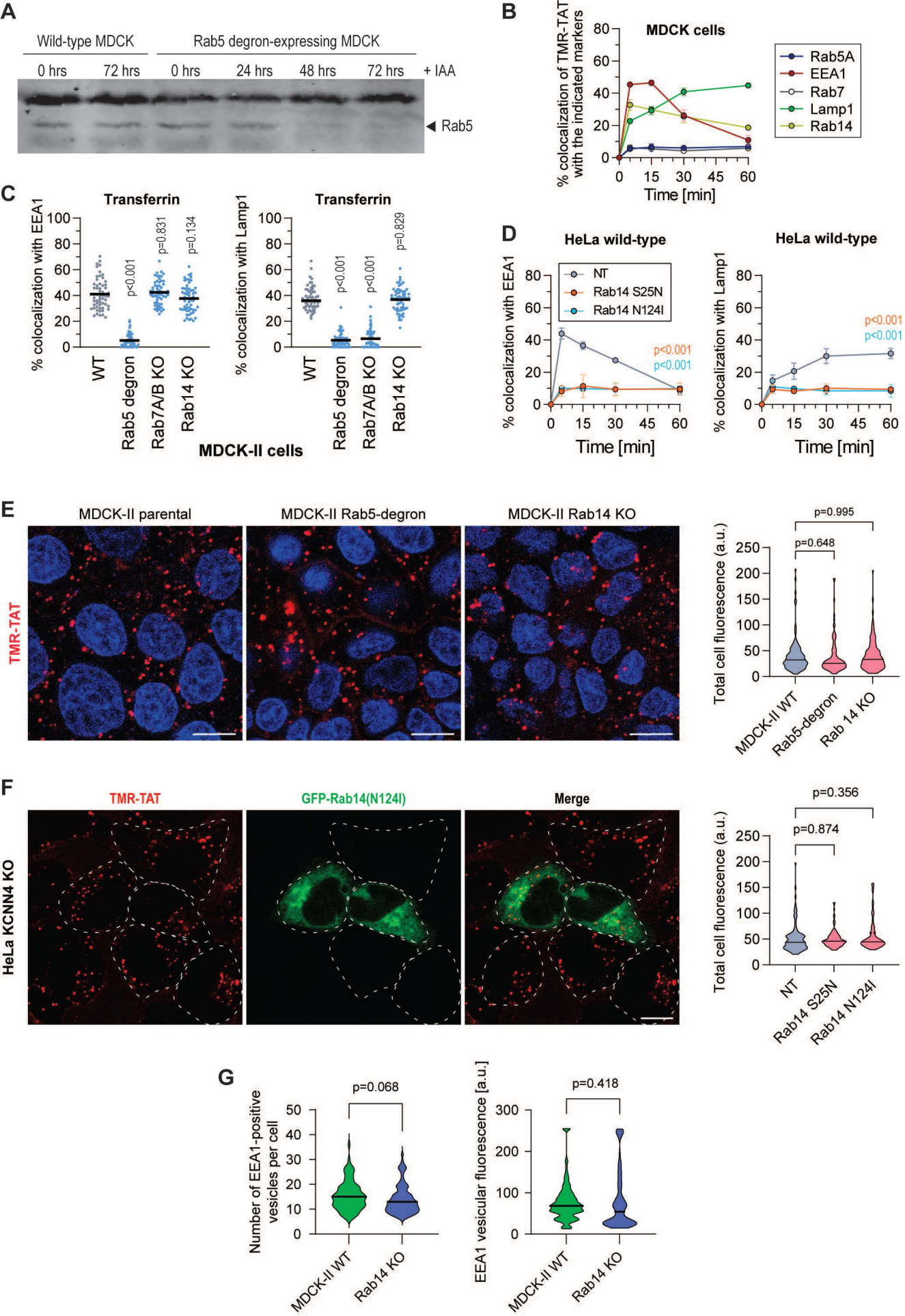
Figure S4. The effect of pan-PI3K inhibitors on cytosolic distribution of endocytosed material and endosomal markers. Related to Figure 2.

(A) KCNN4 knock-out HeLa cells were incubated in serum-free medium for one hour and then incubated 20 minutes in RPMI, 10% serum in the presence or in the absence of 25 μM LY294002. Cells were then lysed and levels of phosphorylated Akt were assessed by Western blotting using a rabbit anti-phospho-AKT antibody (Cell signaling, #92715). Evenness of loading was evaluated by Ponceau S staining.

(B) Representative images of cells incubated with TMR-TAT in the presence or in the absence of pan-PI3K inhibitors. KCNN4 knock-out HeLa cells were preincubated or not for 30 minutes with 25 μM LY294002 or 10 μM wortmannin. TMR-TAT was added for a 5-minute pulse, then washed out and images of live cells were acquired 10 minutes later by confocal microscopy. When used, the pan-PI3K inhibitors were maintained in the media throughout the full duration of the experiment. Images such as shown in this panel were used for the quantitation presented in Figure 2. Scale bar: 10 μm .

(C) Effect of pan-PI3K inhibitors on EEA1 subcellular location. Cells were treated as in panel B but in the absence of TMR-TAT. This corresponds to the 15-minute time point in Figure 2A. Scale bar: 10 μm .

(D) The quantitation of the effect of pan-PI3K inhibitors on EEA1 subcellular location was performed on images acquired in panel C. Cytosolic EEA1 signal was measured using ImageJ by selecting regions of identical surface devoid of endosomes. The results are derived from the analysis of 155-158 cells per condition derived from three independent experiments. Statistical analysis was done with ANOVA multiple comparison with Dunnet's correction.



(legend on next page)

Figure S5. CPP endocytosis in MDCK-II cells. Related to Figure 3.

(A) Western blot-mediated Rab5 detection in lysates of wild-type or Rab5-degron MDCK-II cell incubated with 1 $\mu\text{g/ml}$ doxycycline and 500 μM IAA for the indicated periods of time.

(B) Colocalization of TAT-containing vesicles with the indicated endosomal markers. Wild-type MDCK-II cells were incubated with 40 μM TMR-TAT for 5 minutes and then visualized by live confocal microscopy. A total of 160-178 cells per condition, derived from three independent experiments, were analyzed.

(C) Colocalization quantitation between AlexaFluor647-transferrin and GFP-EEA1 (15 minutes) or Lamp1-GFP (30 minutes) in a pulse chase experiment performed in wild-type MDCK-II cells and the corresponding Rab knock-outs. Per condition, 55-59 cells were analyzed. Statistical analysis was performed with ANOVA multiple comparison to the wild-type cell condition with Dunnett's correction.

(D) Colocalization quantitation between TAT and EEA1 or Lamp1 in cells transfected with Rab14 dominant-negative constructs in wild-type HeLa cells in a pulse chase experiment setting (see Fig. S1D). The data correspond to the mean \pm SD of 150-162 cells per condition derived from three independent experiments. Statistical analysis was performed on AUC values using ANOVA test with Dunnett's correction. The p-values correspond to the comparison with non-transfected (NT) cells.

(E) Left: representative confocal images of the indicated MDCK-II cell lines incubated with 40 μM TMR-TAT for 5 minutes, washed and then imaged 10 minutes later. Scale bar: 10 μm . Right: quantitation of total TMR-TAT uptake based on confocal images in the left panel (130-138 cells were analyzed per condition derived from three independent experiments). Statistical analysis was done with ANOVA multiple comparison with Dunnett's correction.

(F) Left: representative confocal images of KCNN4 knock-out HeLa cells transfected with the dominant-negative GFP-Rab14 (N124I) construct and incubated with 40 μM TMR-TAT for 5 minutes, washed and then imaged 10 minutes later. Scale bar: 10 μm . Right: quantitation of total TMR-TAT uptake based on confocal images in the left panel (145-150 cells were analyzed per condition derived from three independent experiments). Statistical analysis was done with ANOVA multiple comparison with Dunnett's correction.

(G) Quantitation of the number of EEA1-positive vesicles and their fluorescence based on confocal images in wild-type and Rab14 knockout MDCK-II cells. The results are derived from the analysis of 155-163 cells (per condition) taken from three independent experiments. Statistical analysis was done using parametric two-tailed unpaired t-test.

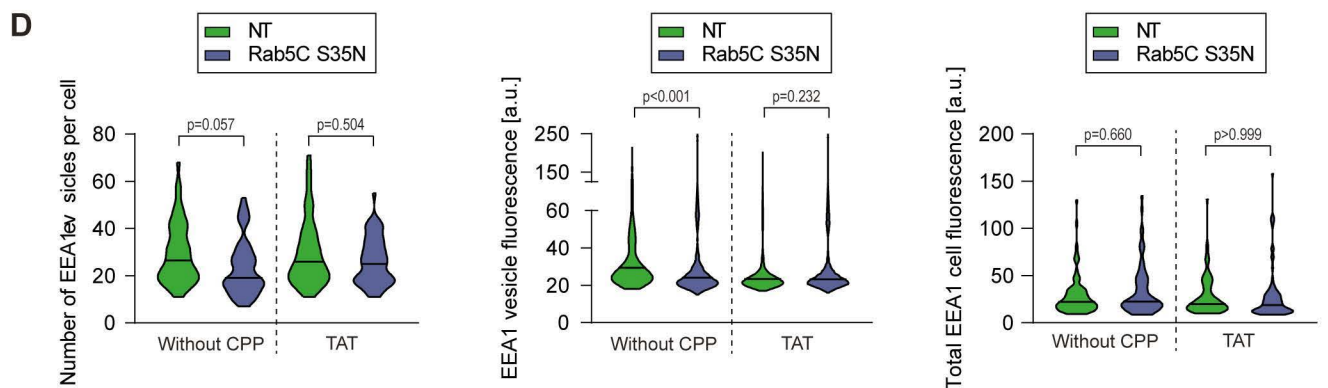
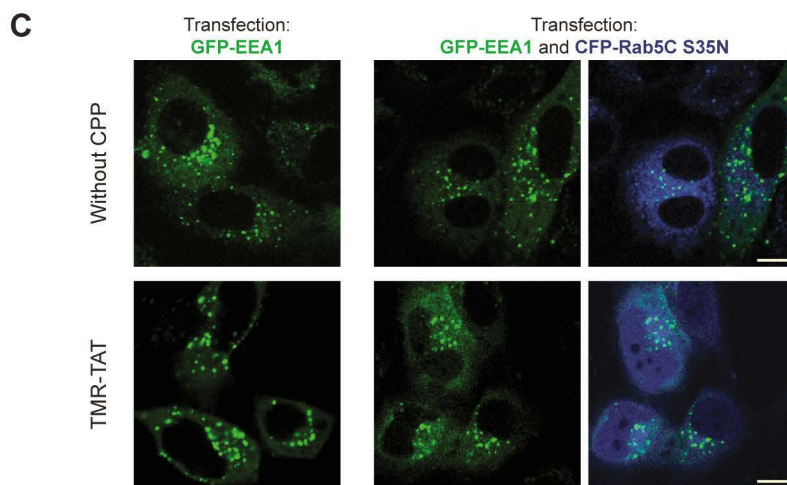
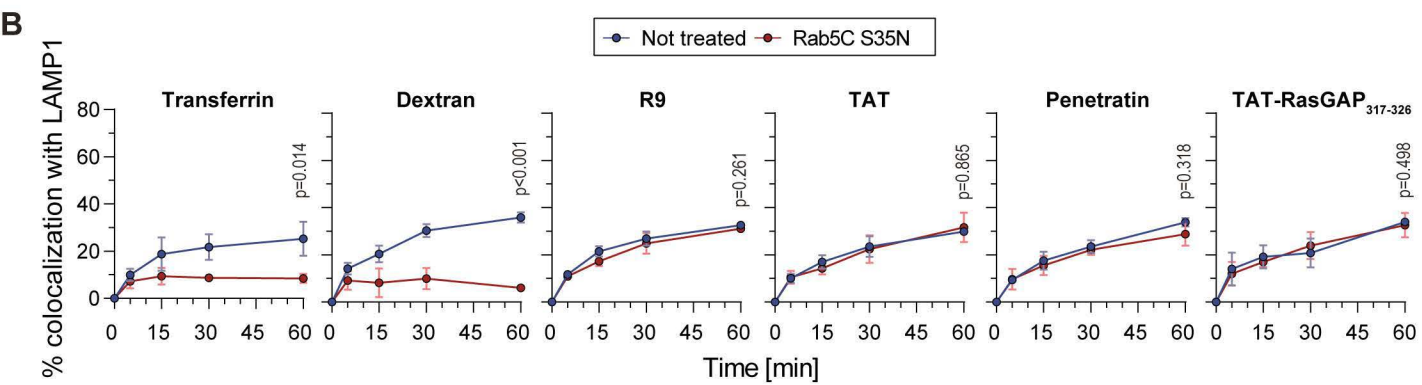
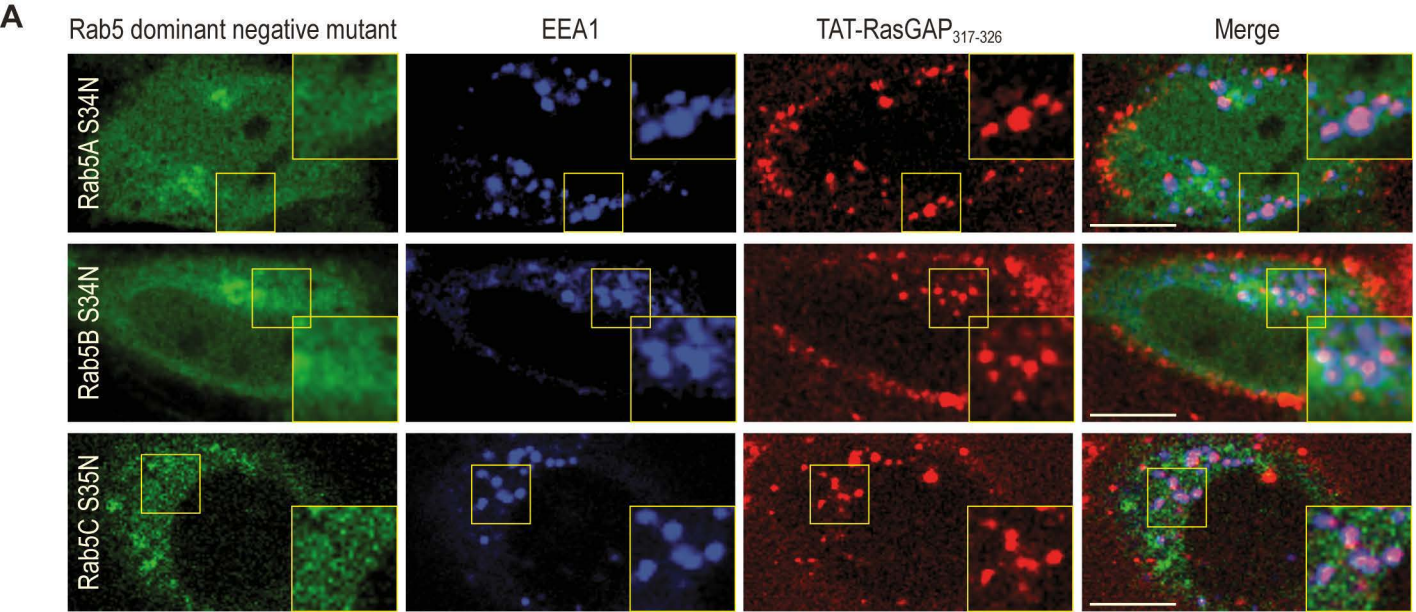


Figure S6. Rab5 is not involved in the maturation of CPP-containing endosomes. Related to Figures 3 and 4.

(A) Representative confocal images of the cells analyzed in Figure 4B. Scale bar: 10 μm .

(B) Colocalization quantitation of transferrin, dextran, and the indicated CPPs with Lamp1 in cells transfected with a Rab5C dominant-negative construct in KCNN4 knockout HeLa cells using a pulse-chase experiment setting (see Fig. S1D). The data correspond to the mean \pm SD of 166-172 cells analyzed per condition, derived from three independent experiments. Statistical analysis was performed using parametric two-tailed t-test based on AUC values.

(C) Representative confocal images of GFP-EEA1-transfected KCNN4 knockout HeLa cells co-transfected or not with a CFP-Rab5C S35N dominant-negative construct. Cells were incubated or not with 40 μM TMR-TAT for 5 minutes and then imaged 10 minutes later. Scale bar: 10 μm .

(D) Quantitation of the number of EEA1-positive vesicles and their fluorescence, as well as total EEA1 cell fluorescence (cytosolic and vesicular) on images such as shown in panel C. A total of 150-155 cells per condition, derived from three independent experiments, were analyzed. Statistical analysis was done using ANOVA multiple comparison with Tuckey correction.

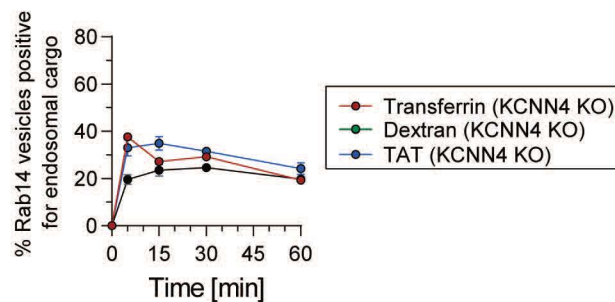
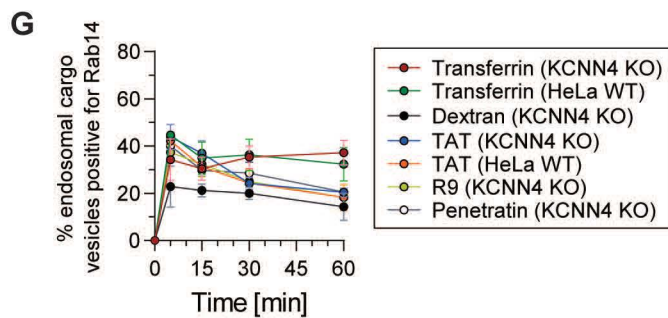
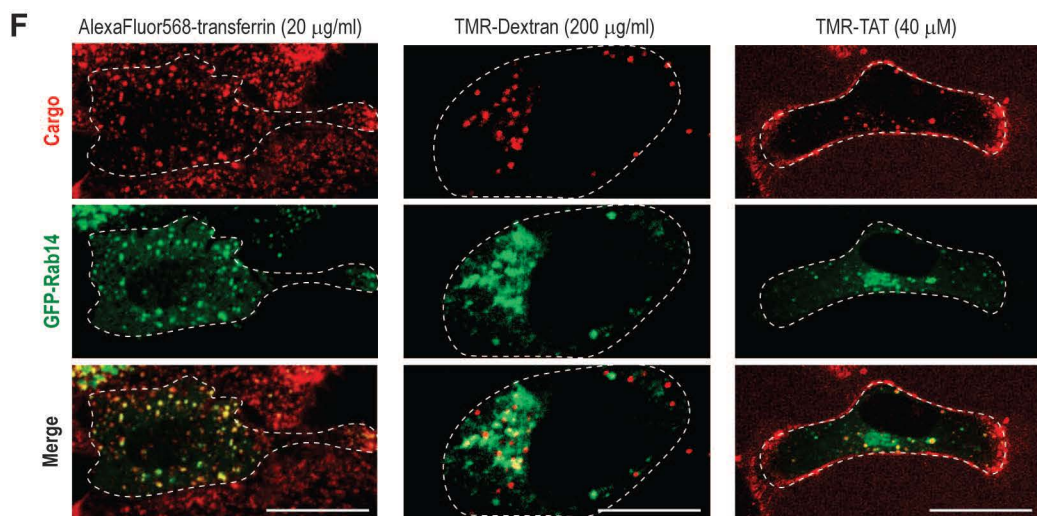
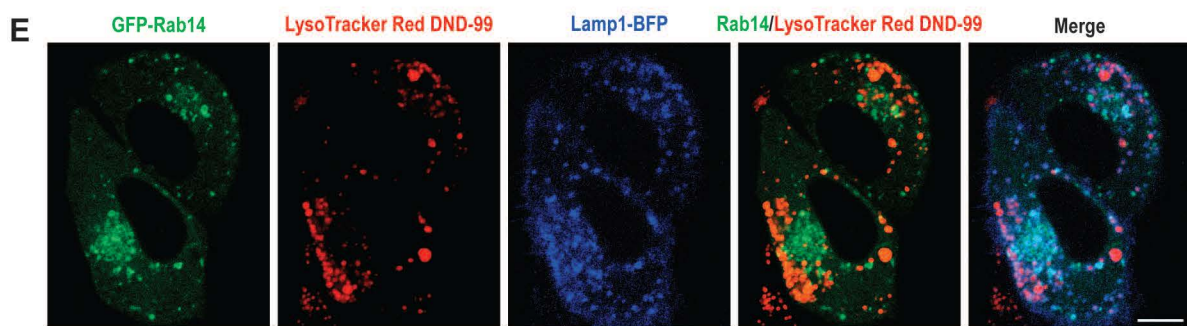
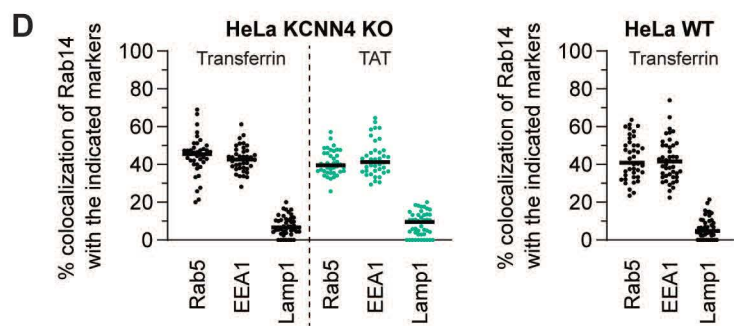
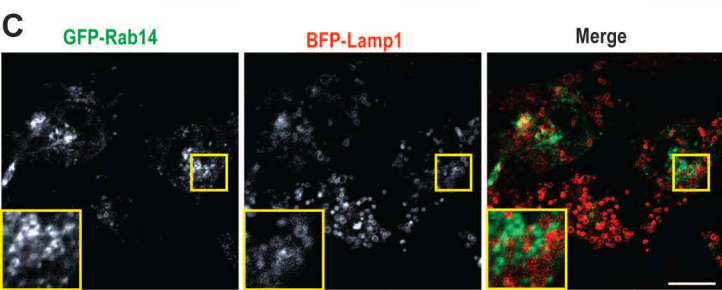
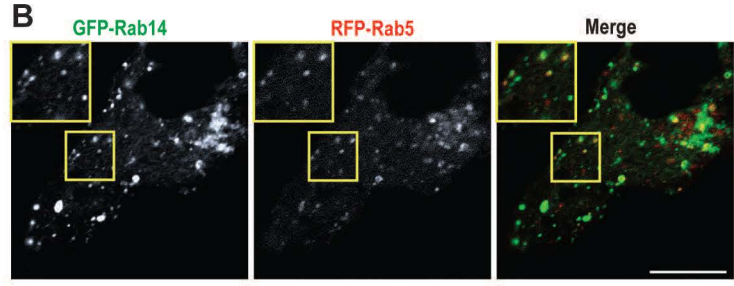
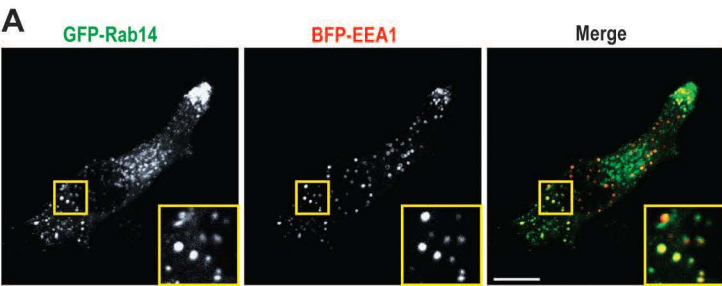


Figure S7. Rab14 is not a specific marker for the CPP endocytic pathway. Related to Figure 7.

(A) Representative confocal images of KCNN4 knockout HeLa cells ectopically expressing GFP-Rab14 and BFP-EEA1 that were incubated for 5 minutes with 40 μ M TMR-TAT. Images were acquired at 30 minutes post-incubation with TMR-TAT. Scale bar: 10 μ m.

(B) Representative confocal images of KCNN4 knockout HeLa cells ectopically expressing GFP-Rab14 and RFP-Rab5A that were incubated for 5 minutes with 40 μ M unlabeled TAT. Images were acquired at 30 minutes post-incubation with TAT. Scale bar: 10 μ m.

(C) Representative confocal images of KCNN4 knockout HeLa cells ectopically expressing GFP-Rab14 and Lamp1-BFP that were incubated for 5 minutes with 40 μ M TMR-TAT. Images were acquired 30 minutes post-CPP addition. Scale bar: 10 μ m.

(D) Colocalization quantitation of Rab14 with the indicated endosomal markers in wild-type and KCNN4 knockout HeLa cells incubated for 5 minutes with 20 μ g/ml AlexaFluor647-transferrin or 40 μ M TMR-TAT. A total of 54-60 cells per condition were analyzed.

(E) Representative confocal images of KCNN4 knockout HeLa cells expressing GFP-Rab14 and Lamp1-BFP. The images were acquired after one hour of incubation with LysoTracker Red DND-99 (50 nM). Scale bar: 10 μ m.

(F) Representative confocal images of KCNN4 knockout HeLa cells expressing GFP-Rab14, incubated with the indicated cargos for 5 minutes, and imaged 10 minutes later. Scale bar: 10 μ m.

(G) Colocalization quantitation between the indicated endocytosed material and GFP-Rab14 ectopically expressed in wild-type and KCNN4 knockout HeLa cells. The results correspond to the mean \pm SD of three independent experiments. Left: the colocalization quantitation corresponds to the percentage of endosomes positive for both GFP-Rab14 and the indicated endocytosed material over the total number of vesicles positive for the endocytosed material. Right: the colocalization quantitation corresponds to the percentage of endosomes positive for both GFP-Rab14 and the indicated endocytosed material over the total number of Rab14-positive vesicles. A total of 140-150 cells per condition were analyzed.